

1
2
3
4
5
6
7
8
9
10
11
12
13
14
15
16
17
18
19
20
21
22
23
24
25
26
27
28
29
30
31
32
33
34
35
36

Constraining Black Carbon Aerosol over Asia using OMI Aerosol Absorption Optical Depth and the Adjoint of GEOS-Chem

**Li Zhang^{1,2}, Daven K. Henze¹, Georg A. Grell², Gregory R. Carmichael³, Nicolas
Bousserez¹, Qiang Zhang⁴, Omar Torres⁵, Changwoo Ahn⁶, Zifeng Lu⁷, Junji
Cao⁸, Yuhao Mao^{9,10}**

¹Department of Mechanical Engineering, University of Colorado, Boulder, CO, USA

²Global Systems Division, Earth System Research Laboratory, NOAA, Boulder, CO,
USA

³Department of Chemical and Biochemical Engineering, University of Iowa, Iowa, IA,
USA

⁴Center for Earth System Science, Tsinghua University, Beijing, China

⁵NASA Goddard Space Flight Center, Greenbelt, MD, USA

⁶Science Systems and Applications, Inc., Lanham, MD, USA

⁷Decision and Information Sciences Division, Argonne National Laboratory, Argonne,
IL, USA

⁸Key Lab of Aerosol Chemistry & Physics, Institute of Earth Environment, Chinese
Academy of Sciences, Xi'an, China

⁹Department of Atmospheric and Oceanic Sciences, University of California, Los
Angeles, CA, USA

¹⁰State Key Laboratory of Atmospheric Boundary Layer Physics and Atmospheric
Chemistry, Institute of Atmospheric Physics, Chinese Academy of Sciences, Beijing,
China

Submitted to Atmospheric Chemistry and Physics

February 2015

*Corresponding author:
daven.henze@colorado.edu
Dept. of Mechanical Engineering
1111 Engineering Drive ECES 114
University of Colorado, Boulder
Boulder, CO 80309

1 **Abstract**

2 Accurate estimates of the emissions and distribution of black carbon (BC) in the
3 region referred to here as Southeastern Asia (70°E–150°E, 11°S–55°N) are critical to
4 studies of the atmospheric environment and climate change. Analysis of modeled BC
5 concentrations compared to in situ observations indicates levels are underestimated
6 over most of Southeast Asia when using any of four different emission inventories.
7 We thus attempt to reduce uncertainties in BC emissions and improve BC model
8 simulations by developing top-down, spatially resolved, estimates of BC emissions
9 through assimilation of OMI observations of aerosol absorption optical depth
10 (AAOD) with the GEOS-Chem model and its adjoint for April and October of 2006.
11 Overwhelming enhancements, up to 500%, in anthropogenic BC emissions are shown
12 after optimization over broad areas of Southeast Asia in April. In October, the
13 optimization of anthropogenic emissions yields a slight reduction (1~5%) over India
14 and parts of southern China, while emissions increase by 10~50% over eastern China.
15 Observational data from in situ measurements and AERONET observations are used
16 to evaluate the BC inversions and assess the bias between OMI and AERONET
17 AAOD. Low biases in BC concentrations are improved or corrected in most eastern
18 and central sites over China after optimization, while the constrained model still
19 underestimates concentrations in Indian sites in both April and October, possibly as a
20 consequence of low prior emissions. Model resolution errors may contribute up to a
21 factor of 2.5 to the underestimate of surface BC concentrations over northern India.
22 We also compare the optimized results using different anthropogenic emission
23 inventories and discuss the sensitivity of top-down constraints on anthropogenic
24 emissions with respect to biomass burning emissions. In addition, the impacts of
25 different observation operators and a priori constraints on the optimization are
26 investigated. Overall, despite these limitations and uncertainties, using OMI AAOD to
27 constrain BC sources improves model representation of BC distributions, particularly
28 over China.
29

1

2 **1. Introduction**

3 Black carbon (BC) is a product of incomplete combustion of carbonaceous fuels,
4 enhanced concentrations of which have led to a present-day overall positive radiative
5 forcing and climate warming [Charlson and Pilat, 1969; Satheesh and Ramanathan,
6 2000; Bond et al., 2013]. More than ten years ago, Jacobson [2000] and Hansen et al.
7 [2000] recognized that preindustrial to present increases in BC might warm the
8 atmosphere about one third as much as CO₂. Recently, an assessment report by Bond
9 et al. [2013] indicates that the global average preindustrial to present radiative forcing
10 from BC is +1.1 W/m² with 90% uncertainty bounds of +0.17 to +2.1 W/m², which is
11 more than two thirds that of CO₂ (+1.56 W/m²). Additionally, BC aerosols constitute
12 up to 10-15% of the mass concentration of fine particulate matter (PM_{2.5}) over
13 continental regions, exposure to which is known to adversely effect human health
14 [e.g., Janssen et al., 2005; Schwartz et al., 2008; Janssen et al., 2011; Li et al., 2014].
15 Given the magnitude of BC climate effects and health impacts, a number of studies
16 have investigated its direct effect [Forster 2007; Ramanathan and Carmichael, 2008],
17 semi-direct effect [Ackeman et al., 2000; Johnson et al., 2004], indirect effect [Cozic
18 et al., 2007; Liu et al., 2009; Oshima et al., 2009], and the albedo effect when
19 deposited on snow [Hansen and Nazarenko, 2004; Hansen et al., 2005; Flanner et al.,
20 2007; Qian et al., 2009] using various numerical models and observations.
21 Central estimates of global annual emissions of BC are 8.0 Tg, of which 38% comes
22 from fossil fuel, 20% from biofuel and 42% from open burning [Bond et al., 2004].
23 At the same time, estimates of BC emissions are recognized as having large

1 uncertainties -- 50% at global scales and a factor of two to five at regional scales
2 [Bond et al., 2004; Ramanathan and Carmichael, 2008]. The Asian region referred to
3 here as Southeast Asia (70°E–150°E, 11°S–55°N) is the major anthropogenic BC
4 source region in the world, with growth in BC emissions of 21% over China and 41%
5 over India from 1996 to 2010 associated with rapid economic and industrial
6 development [Lu et al., 2011]. BC emissions from both energy-related combustion
7 and biomass burning that occur largely in Asia and Africa currently appear
8 underestimated [Bond et al., 2013]. A global top-down estimate of BC emission using
9 AERONET observation by Cohen and Wang [2014] indicated that commonly used
10 global BC emissions datasets may be underestimated by a factor of two or more.
11 Sixteen models from the AeroCom aerosol model intercomparisons underestimated
12 the Southeast Asian BC surface concentrations by a factor of 2~3 [Koch et al., 2009].
13 The GEOS-Chem model also underestimated monthly BC concentrations at almost all
14 rural sites in China, particularly in January 2006, which indicated a regional
15 underprediction of carbonaceous aerosol sources associated with anthropogenic
16 activities [Fu et al., 2012; Wang et al., 2013]. In addition, the global atmospheric
17 absorption attributable to BC is too low in many global aerosol models by a factor of
18 almost three on a global mean basis, which can be attributed to the models lacking
19 treatment of enhanced absorption caused by mixing of BC with other constituents and
20 the amount of BC in the atmosphere [Koch et al., 2009; Bond et al., 2013]. On the
21 other hand, a typical fresh particle mass absorption cross section (MABS, essentially
22 the column BC absorption divided by the load) of about $7.5 \text{ m}^2 \text{ g}^{-1}$ recommended by

1 Bond and Bergstrom [2006] is not represented in most models, which should
2 probably increase as particles age [Koch et al., 2009]. This bias would also impact
3 simulated AAOD, and inferences about emissions based on such comparisons would
4 likewise be biased.

5 To reduce uncertainties in BC emissions and improve poor representation of BC in
6 model simulations, different top-down approaches have been used to constrain bottom
7 up BC emissions, such as the linear constraints between concentrations and emissions
8 [Park et al., 2003; Kondo et al., 2011; Fu et al., 2012; Wang et al., 2013], inverse
9 modeling using the decoupled direct method [Hu et al., 2009a; Hu et al., 2009b], the
10 Kalman filter technique [Cohen and Wang 2014], and the adjoint based 4D variational
11 approach [Hakami et al., 2005]. These studies have exclusively used in situ
12 measurements or airborne observations, which can provide accurate observations of
13 aerosol properties. However, they are often incomplete in their spatial or temporal
14 coverage. Satellite measurements of aerosol optical depth (AOD) have much broader
15 temporal and spatial coverage, and have also been used to constrain BC sources
16 [Huneeus et al., 2003; Xu et al., 2013]. However, AOD reflects the contribution from
17 all aerosol components, making it difficult to distinguish and quantify different
18 aerosol species, especially their relative fractions.

19 The OMI aerosol absorption optical depth (AAOD), the non-scattering part of the
20 AOD, is an atmospheric column measurement of absorbing aerosol particles, i.e.,
21 absorbing carbon and mineral dust, which provides a different perspective to
22 constrain BC sources [Torres et al., 1998; Koch et al., 2009]. In this study, the

1 GEOS-Chem adjoint model and satellite observations of OMI AAOD are used to
2 constrain spatially resolved BC emissions. Our study will focus on April and October
3 to compare times when the dust loading is relatively large and small over Southeast
4 Asia. Section 2 describes the observations, emissions, and forward and inverse model
5 used in this study. Then we quantify discrepancies between observations and model
6 estimates based on different BC anthropogenic emissions in Section 3. Section 4
7 describes how formulation of the inverse problem affects the results; evaluation of the
8 inversion results with different prior emission inventories and independent
9 observations are presented in Section 5, and we end with discussion and conclusions
10 in Section 6.

11

12 **2. Data and Models**

13 **2.1 Observations**

14 **2.1.1 OMI AAOD**

15 The Ozone Monitoring Instrument (OMI) aboard Aura is a nadir-viewing, wide-swath
16 hyper-spectral imaging spectrometer that provides daily global coverage with high
17 spectral resolutions and spatial resolution of $13 \times 24 \text{ km}^2$ at nadir [Levelt et al.,
18 2006a]. It detects backscattered solar radiance in the ultraviolet-visible wavelengths
19 (0.27 to 0.5 μm) to measure aerosols, clouds, surface UV irradiance, and trace gases
20 [Levelt et al., 2006b]. OMI takes advantage of the greater sensitivity of radiances
21 measured at the top-of-atmosphere in the near-UV region to the varying load and type
22 of aerosols to derive extinction AOD, single scattering albedo (SSA), and AAOD

1 using an inversion procedure at 354, 388 and 500 nm generated by the near-UV
2 (OMAERUV) algorithm [Torres et al., 2007]. The optical depths at 388 nm are
3 inverted from radiance observations while the 354 and 500 nm results are obtained by
4 conversion of the 388 nm retrievals. The OMAERUV retrieval algorithm is
5 particularly sensitive to carbonaceous and mineral aerosols. The OMAERUV retrieval
6 algorithm assumes that the column aerosol load can be represented by one of three
7 types of aerosols and uses a set of aerosol models to account for the presence of these
8 aerosols: carbonaceous aerosol from biomass burning, desert dust, and light absorbing
9 sulfate-based aerosols. Each aerosol type is represented by seven aerosol models of
10 varying single scattering albedo, for a total of twenty-one models. The twenty-one
11 aerosol models used by OMAERUV are based on long-term statistics of ground-based
12 observations by the AERONET. Due the large sensitivity of the OMI near UV
13 observations to particle absorption, the AAOD is the most reliable quantitative
14 OMAERUV aerosol parameter, especially over land. The root-mean-square error for
15 AAOD is estimated to be $\sim 0.01^1$.

16 Since the retrieval algorithm is sensitive to the aerosol height, the Level 2 OMI
17 AAOD data reports a set of retrieved parameters for different assumptions of the
18 altitude of the aerosol center of mass: at the surface, and at 1.5, 3.0, 6.0 and 10.0 km
19 above the surface [Torres et al., 2005]. For carbonaceous and desert dust particles, the
20 aerosol load is assumed to be vertically distributed following a Gaussian function
21 characterized by peak (aerosol layer height) and half-width (aerosol layer geometric

¹daac.gsfc.nasa.gov/Aura/data-holdings/OMI/documents/v003/OMAERUV_README_V003.doc

1 thickness) values [Torres et al., 2005; Torres et al., 2013]. The retrieval values of
2 AAOD are much larger if using the aerosol layer altitude where more absorbing
3 aerosols are loaded. In general, when comparing satellite retrievals of trace gases with
4 other measurements or model simulations, it is essential to take into account the
5 different sensitivities of the instruments by applying averaging kernels [Luo et al.,
6 2007; Worden et al., 2007]. However, there is no averaging kernel for OMI
7 AOD/AAOD retrievals. It is thus important to consider differences in aerosol
8 properties and distributions used in the retrieval algorithm with those in the
9 assimilation model (e.g., GEOS-Chem). The retrieval “Final AAOD” products are
10 interpolated values using the aerosol layer height value given by the Cloud-Aerosol
11 Lidar with Orthogonal Polarization (CALIOP) climatology as the retrieval algorithm
12 is sensitive to aerosol layer height [Torres et al., 2013]. In order to obtain a consistent
13 vertical profile between the OMI retrieval and GEOS-Chem, we use the GEOS-Chem
14 simulated aerosol layer height instead of the CALIOP-based aerosol layer height
15 climatology to calculate a GEOS-Chem-based OMI AAOD (OMI_GC AAOD) as a
16 linear interpolation of the OMI AAOD values corresponding to different assumed
17 peak heights. Figure 1 shows the differences between OMI_Final and OMI_GC
18 AAOD over Southeast Asia for April and October 2006. In April, the enhancements
19 from applying the GEOS-Chem aerosol layer height are quite significant, with 30-
20 50% increases over eastern China and downwind areas while 20-30% increases over
21 India and southeastern Asia, since the simulated aerosol layer heights are much lower
22 than those based on CALIOP. The increases even exceed 60% across broad areas over

1 the tropical ocean. Some reductions are shown over parts of western China and
2 northern Asia in the OMI_GC AOD. In October, the patterns of enhancement and
3 reduction are similar to those in April, with smaller changes (less than 20%) over
4 broad continental areas. The most significant differences occur near the major aerosol
5 source regions, such as eastern China and South Asia.

6 **2.1.2 AERONET AOD**

7 The Aerosol Robotic Network (AERONET) is a ground-based instrument network
8 providing a long-term, continuous and readily accessible public domain database of
9 aerosol optical, microphysical and radiative properties [Holben et al., 1998].
10 AERONET inversion code provides aerosol optical properties (including size
11 distribution, refractive index, and single scattering albedo) in the total atmospheric
12 column derived from the direct and diffuse radiation measured by Cimel sun/sky-
13 radiometers [Dubovik and King, 2000; Dubovik et al., 2000, 2002a, 2002b; Dubovik
14 et al., 2006; Sinyuk et al., 2007].

15 We use Level 2.0 quality-assured AERONET aerosol inversions data of AOD at 440
16 nm. The prefield and postfield calibrations have been applied in these measurements
17 and they were cloud cleared and manually inspected [Omar et al., 2013]. The total
18 uncertainty in the AERONET AOD for field instruments is ± 0.1 to ± 0.2 and is
19 spectrally dependent with the higher errors (± 0.2) in the UV spectral range [Eck et al.,
20 1999]. The retrieved single scattering albedo uncertainties were within 0.03,
21 estimated by Dubovik et al., [2000], with the exception of the 0.44 μm retrievals for
22 the desert dust case when they increased by ~ 0.09 and 0.07 for low and high aerosol

1 loadings, respectively [Sinyuk et al., 2007].

2 **2.1.3 In situ measurements**

3 For the monthly surface BC observation over Southeast Asia, we combine the in situ
4 measurements of BC concentration based on several published studies [Zhang et al.,
5 2008; Beegum et al., 2009; Moorthy et al., 2013]. Over China, the monthly surface
6 BC concentrations are from 12 sites, including urban sites and rural sites for April and
7 October, 2006, which were based on results of Zhang et al. [2008]. The locations of
8 these 12 sites are shown in Fig. 2. The BC concentrations are analyzed using thermo-
9 chemical analysis from PM₁₀ aerosols, which were collected by air sample [Zhang et
10 al., 2008]. The daily BC measurements are only available at the site of Xi'an (XIA).
11 The PM_{2.5} BC concentrations were measured continuously as 5-min averages by
12 quartzfiber filter tape transmission at an 880 nm wavelength with an aethalometer
13 [Hansen et al., 1984]. More details about the measurement methods are described by
14 Cao et al. [2007; 2009].

15 The measurements of monthly surface BC concentrations for 2006 using
16 aethalometers over India were based on Beegum et al. [2009] and Moorthy et al.
17 [2013], which were carried out in eight sites (see Table 1) covering India and adjacent
18 oceanic regions. Locations of these sites are indicated in Fig. 2. More details about
19 the measurements and sites are described by Beegum et al. [2009]. DEL and KGP
20 represent urban and semi-urban sites in the Indo-Gangetic Plain (IGP). HYD and
21 PUN represent urban locations. TVM is a semi-urban coastal station in the south

1 India; NTL is a high altitude location in the central Himalayas, and MCY and PBR
2 are two island locations representing the Arabian Sea and Bay of Bengal, respectively.

3 **2.2 GEOS-Chem**

4 GEOS-Chem is a global three-dimension chemical transport model driven by
5 assimilated meteorological observations from the Goddard Earth Observing System
6 (GEOS) of the NASA Global Modeling and Assimilation Office (GMAO) [Bey et al.,
7 2001]. We use the nested-grid GEOS-Chem model [Wang et al., 2004; Chen et al.,
8 2009] driven by GEOS-5 meteorological fields with 6-hour temporal resolution (3-
9 hour for surface variables and mixing depths), 0.5° (latitude) \times 0.667° (longitude)
10 horizontal resolution over the window of Southeast Asia (70°E – 150°E , 11°S – 55°N),
11 and 47 vertical layers between the surface and 0.01 hPa. A global simulation with
12 lower resolution of 4° (latitude) \times 5° (longitude) provides the lateral boundary
13 conditions to the higher resolution nested-grid simulation every 3 hours.

14 The original carbonaceous aerosol simulation in GEOS–Chem was developed by Park
15 et al. [2003]. It assumes that 80% of BC and 50% of OC emitted from primary
16 sources are hydrophobic and that hydrophobic aerosols become hydrophilic with an e-
17 folding time of 1.15 days [Park et al., 2003; Chin et al., 2002; Cooke et al., 1999].
18 Dust in GEOS-Chem is distributed across four size bins (radii 0.1– 1.0, 1.0–1.8, 1.8–
19 3.0, and 3.0–6.0 μm) following Ginoux et al. [2004]. The smallest size bin is further
20 divided equally into four sub-micron size bins (with effective radii centered at 0.15,
21 0.25, 0.4 and 0.8 μm) for calculation of optical properties and heterogeneous
22 chemistry [Fairlie et al., 2010; Ridley et al., 2012]. Due to the significant positive

1 biases identified in GEOS-Chem dust simulations both in surface concentration and
2 dust AOD [Fairlie et al., 2010, Ku and Park, 2011; Ridley et al., 2012; Wang et al.,
3 2012], a new emitted dust particle size distribution (PSD) based upon scale-invariant
4 fragmentation theory [Kok, 2011] with constraints from in situ measurements [Zhao
5 et al., 2010] is implemented in GEOS-Chem to improve the dust simulation [Zhang et
6 al., 2013]. Large discrepancies are reduced between the simulated surface-level fine
7 dust concentration and measurements from the IMPROVE network in the western US
8 during March to May of 2006 [Zhang et al., 2013]. The new PSD also improves the
9 positive biases of AOD over the Asian and African dust source region in April 2006
10 (See Fig. S1 in supplemental). The wet deposition scheme [Liu et al., 2001] includes
11 scavenging in convective updrafts as well as in-cloud and below-cloud scavenging
12 from convective and large-scale precipitation. Dry deposition is based on the
13 resistance-in-series scheme of Wesely [1989] as implemented by Wang et al. [1998].
14 The aerosol optical depth at 400 nm is calculated online assuming log-normal size
15 distributions of externally mixed aerosols and is a function of the local relative
16 humidity to account for hygroscopic growth [Martin et al., 2003]. The AAOD of each
17 aerosol species is calculated as [Ma et al., 2012; Cohen and Wang, 2014; Cohen,
18 2014]

$$19 \quad \text{AAOD} = \text{AOD} * (1 - \text{SSA}) \quad (1),$$

20 where SSA is the single scattering albedo.

21 **2.3 BC Emission Inventories**

22 Emissions of BC from biomass burning sources are taken from version 2 of the GFED

1 8-day inventory [van der Werf et al., 2006; Randerson et al., 2006]. GFED v2 is
2 derived using satellite observations of active fire counts and burned areas in
3 conjunction with the Carnegie-Ames-Stanford-Approach (CASA) biogeochemical
4 model. Carbon emissions are calculated as the product of burned area, fuel load and
5 combustion completeness. Burned area is derived using the active fire and 500-meter
6 burned area datasets from the Moderate Resolution Imaging Spectroradiometer
7 (MODIS) as described by Giglio et al. [2006]. We also use a newer version of GFED
8 v3 daily emissions for sensitivity analysis [van derWerf et al., 2010]. Compared to
9 GFED v2, the main update in GFED v3 is the spatial resolution of the global grid is
10 quadrupled from 1° to 0.5°, the native 500-m MODIS daily burned area maps are
11 applied [Giglio et al., 2010], the regional regression trees of GFEDv2 are replaced by
12 a local regression approach in producing the indirect, active-fire based estimates of
13 burned area, and a revised version of Carnegie-Ames Stanford Approach (CASA)
14 biogeochemical model is used.

15 Global anthropogenic emissions for carbonaceous aerosols (BC/OC) in GEOS-Chem
16 are originally from Bond et al. [2004, 2007], which contain both biofuel and fossil
17 fuel emissions. The estimated BC emissions uncertainties are -36% to 149% over
18 China and 38% to -119% for India [Bond et al., 2004; Lu et al., 2011]. In this study,
19 we evaluate three additional carbonaceous anthropogenic emission inventories over
20 Southeast Asia and China: the Streets regional inventory for Intercontinental
21 Chemical Transport Experiment - Phase B (INTEX-B), the Southeast Asia
22 Composition, Cloud, Climate Coupling Regional Study (SEAC⁴RS) emission

1 inventory, and the Multi-resolution Emission Inventory for China (MEIC,
2 <http://www.meicmodel.org/>). Anthropogenic emissions are all classified into four
3 major sectors: power generation, industry, residential and transport. The INTEX-B
4 inventory is based on 2006 and contains monthly variations with $0.5^\circ \times 0.5^\circ$
5 horizontal resolution over Southeast Asia (Zhang et al., 2009). The SEAC⁴RS
6 inventory is an annual, finer resolution inventory based on 2012, with $0.1^\circ \times 0.1^\circ$
7 horizontal resolution over Southeast Asia [Lu et al., 2011]. The average uncertainties
8 of BC are estimated to be -43% to 90% over China, which are much lower than those
9 of the INTEX-B between -68% to 308% [Zhang et al., 2009; Lu et al., 2011]. The
10 MEIC emission inventory over China also includes monthly variations and is
11 provided at the $0.5^\circ \times 0.5^\circ$ horizontal resolution. These four anthropogenic emission
12 inventories are regridded to the GEOS-Chem resolution of $0.5^\circ \times 0.667^\circ$, and their
13 annual emissions are shown in Fig. 3. The differences in these inventories exceed
14 100% across broad areas, especially over India and eastern China. The anthropogenic
15 emission inventory of INTEX-B is comparable to that of MEIC over eastern China
16 while lower than that of Bond and SEAC⁴RS over western China and India. Both
17 Bond and SEAC⁴RS inventories are lower over central and eastern China compared to
18 those of INTEX-B and MEIC inventories. With much finer resolution, the SEAC⁴RS
19 emission inventory indicates more hot spots spread across eastern and central China
20 and the IGP and eastern India where rural population densities are high and residential
21 coal and biofuel combustion are prevalent [Lu et al., 2011].

22 **2.4 GEOS-Chem Adjoint and Inverse Modeling**

1 An adjoint model is a set of equations auxiliary to a forward model that are used to
2 efficiently calculate the gradient of a scalar model response function with respect to
3 all model parameters simultaneously [Lions, 1971]. The adjoint of GEOS-Chem was
4 developed specifically for inverse modeling including explicit treatment of gas-phase
5 chemistry, heterogeneous chemistry, black and organic primary aerosol, as well as the
6 treatment of the thermodynamic couplings of the sulfate-ammonium-nitrate-formation
7 chemistry [Henze et al., 2007; 2009], with code updates following the relevant parts
8 of the GEOS-Chem forward model up through version v9. The GEOS-Chem adjoint
9 model has been developed and widely used to constrain sources of emission such as
10 dust [Wang et al., 2012], ammonia [Zhu et al., 2013], CO [Kopacz et al., 2009;
11 Kopacz et al., 2010; Jiang et al., 2011], CH₄ [Wecht et al., 2012; Wecht et al., 2014],
12 and to investigate pollution transport [e.g., Zhang et al., 2009, Kopacz et al., 2011].

13 The 4D variational data assimilation technique is used with the GEOS-Chem
14 adjoint model to combine observations and models to calculate an optimal estimate of
15 emissions. A range of emissions are constructed using control variables, σ , to adjust
16 the vector of model emissions via application as scaling factors with elements $\sigma = \frac{E}{E_a}$,
17 where E and E_a are posterior and prior BC emission vectors, respectively. This
18 method of inverse modeling seeks σ that minimizes the cost function, J , presented
19 by:

$$22 \quad J = \frac{1}{2} \sum_{c \in \Omega} (Hc - \mathbf{c}_{obs})^T \mathbf{S}_{obs}^{-1} (Hc - \mathbf{c}_{obs}) + \frac{1}{2} \gamma_r (\sigma - \sigma_a)^T \mathbf{S}_a^{-1} (\sigma - \sigma_a) \quad (2),$$

20 where \mathbf{c} is the vector of species concentrations mapped to the observation space by H ,
21 the observation operator, \mathbf{c}_{obs} is the vector of species observations, σ_a is the prior

1 estimate of the scaling factors, \mathbf{S}_{obs} and \mathbf{S}_a are error covariance estimates of the
2 observations and scaling factors, respectively, and Ω is the domain over which
3 observations are available. The first term of the cost function in Eq. (2) is the
4 observation term, which is the total prediction error incurred for departure of model
5 predictions from the observations. The second term, the a priori term or penalty
6 (background) term, is the penalty incurred for departure from the prior emissions.
7 Here \mathbf{S}_a is assumed to be diagonal, and the significance of the prior information is
8 more of a smoothness constraint than a rigorous estimate of prior uncertainty
9 [Rodgers, 2000]. γ_r is a regularization parameter, which used to balance the two terms
10 [Hansen 1998; Henze et al., 2009]. We will discuss the contributions of the penalty
11 term in Section 4.2.

12 Overall, the minimum value of the cost function balances the objectives of improving
13 model performance while ensuring the model itself remains within a reasonable range
14 (as dictated by \mathbf{S}_a^{-1}) of the initial model. The minimum of the cost function is sought
15 iteratively using the quasi-Newton L-BFGS-B algorithm [Zhu et al., 1994; Byrd et al.,
16 1995]. This approach requires the gradients of the cost function with respect to the
17 emission scaling factors at each iteration, which are calculated with the GEOS-Chem
18 adjoint model.

19 **2.5 Cost function and adjoint forcing**

20 OMI AAOD column observations represent the combined absorption of all aerosols
21 species (dominated by BC, dust, and to a lesser extent OC). Similarly, modeled total
22 column AAOD, \mathbf{T}_{GC} , is the sum of modeled column absorption from BC ($\mathbf{T}_{GC,BC}$), OC

1 (\mathbf{T}_{GC_OC}) and dust (\mathbf{T}_{GC_Dust}):

$$2 \quad \mathbf{T}_{GC} = \mathbf{T}_{GC_BC} + \mathbf{T}_{GC_OC} + \mathbf{T}_{GC_Dust} \quad (3).$$

3 In order to use AAOD observations to develop constraints on BC alone, we must
4 formulate the observation term of the cost function to isolate the impacts of BC on the
5 difference between simulated and observed AAOD. Here we consider four
6 approaches: methods (a) – (d). The first two methods use modeled ratios of BC to
7 total absorption (either in each layer (a), or the total column (b)) to derive an
8 “observed” BC AAOD. Method (c) makes a direct comparison between total AAOD
9 in the model and measurements. Lastly, in method (d), we also consider using a
10 subset of the OMI data that has been flagged in the retrieval process as being
11 impacted by carbonaceous aerosol. These different approaches to constructing a cost
12 function, and the gradient of these cost functions with respect to the vertically
13 resolved modeled BC concentration (i.e., the adjoint forcing) are presented below.
14 Here we do not consider the penalty term in the cost function in order most clearly
15 assess how formulation of the observation term impacts the inversion. The
16 consequences of the different cost function formulations are described in Section 4.1.

17 (a): In this method, the observation term of the cost function can be written as:

$$18 \quad \mathcal{J} = \frac{1}{2} \sum_i^N \sum_{l=1}^L (\tau_{GC_BC,l,i} - \tau_{OMI_BC,l,i})^2 * \mathbf{S}_{OMI,i}^{-2} \quad (4),$$

19 where L is the top of atmosphere, N is the total number of observations, and $\tau_{GC_BC,l,i}$
20 and $\tau_{OMI_BC,l,i}$ are the modeled and observed BC AAODs at layer l for the i^{th}
21 observation, respectively. The latter is calculated for any i from the OMI column
22 AAOD ($\mathbf{T}_{OMI,i}$) using the ratio of vertically resolved BC AAOD to column AAOD in

1 the prior model,

$$2 \quad \tau_{\text{OMI_BC},i} = \mathbf{T}_{\text{OMI},i} \frac{\tau_{\text{GC_BC},i}^a}{\mathbf{T}_{\text{GC},i}^a} \quad (5),$$

3 where superscript a indicates the prior model estimates. Since the ratio $\frac{\tau_{\text{GC_BC},i}^a}{\mathbf{T}_{\text{GC},i}^a}$ is a
4 constant throughout the inversion, the i^{th} adjoint forcing is

$$5 \quad \frac{\partial \mathcal{J}}{\partial \text{BC}_1} = \frac{\partial \tau_{\text{GC_BC},i}}{\partial \text{BC}_1} * \left(\tau_{\text{GC_BC},i} - \mathbf{T}_{\text{OMI},i} \frac{\tau_{\text{GC_BC},i}^a}{\mathbf{T}_{\text{GC},i}^a} \right) * \mathbf{S}_{\text{OMI},i}^{-2} \quad (6).$$

6 (b) In this method, the cost function is based on BC AAOD column differences:

$$7 \quad \mathcal{J} = \frac{1}{2} \sum_i^N (\mathbf{T}_{\text{GC_BC},i} - \mathbf{T}_{\text{OMI_BC},i})^2 * \mathbf{S}_{\text{OMI},i}^{-2} \quad (7).$$

8 The observed BC AAOD column is calculated from the OMI AAOD column and the
9 ratio of modeled column BC AAOD to total column AAOD from the prior simulation:

$$10 \quad \mathbf{T}_{\text{OMI_BC},i} = \mathbf{T}_{\text{OMI},i} \frac{\mathbf{T}_{\text{GC_BC},i}^a}{\mathbf{T}_{\text{GC},i}^a} \quad (8).$$

11 The i^{th} adjoint forcing is thus

$$12 \quad \frac{\partial \mathcal{J}}{\partial \text{BC}_1} = \frac{\partial \tau_{\text{GC_BC},i}}{\partial \text{BC}_1} * \left(\mathbf{T}_{\text{GC_BC},i} - \mathbf{T}_{\text{OMI},i} \frac{\mathbf{T}_{\text{GC_BC},i}^a}{\mathbf{T}_{\text{GC},i}^a} \right) * \mathbf{S}_{\text{OMI},i}^{-2} \quad (9).$$

13 (c) The observation term of the cost function can be written in terms of total column
14 absorption as:

$$15 \quad \mathcal{J} = \frac{1}{2} \sum_i^N (\mathbf{T}_{\text{GC},i} - \mathbf{T}_{\text{OMI},i})^2 * \mathbf{S}_{\text{OMI},i}^{-2} \quad (10).$$

16 In this case, the adjoint forcing is

$$17 \quad \frac{\partial \mathcal{J}}{\partial \text{BC}_1} = \frac{\partial \tau_{\text{GC_BC},i}}{\partial \text{BC}_1} * (\mathbf{T}_{\text{GC_BC},i} + \mathbf{T}_{\text{GC_OC},i} + \mathbf{T}_{\text{GC_Dust},i} - \mathbf{T}_{\text{OMI},i}) * \mathbf{S}_{\text{OMI},i}^{-2} \quad (11).$$

18 (d) The OMI OMAERUV retrievals algorithm also flags instances for which the
19 retrieval algorithm relied upon the presence of carbonaceous aerosols. Using only
20 these retrievals, the observation term of the cost function can be written in terms of
21 the direct difference between simulated columns BC AAOD and flagged OMI AAOD

1 observations:

$$2 \quad J = \frac{1}{2} \sum_i^N (\mathbf{T}_{GC_BC,i} - \mathbf{T}_{OMI_BC_Flag,i})^2 * \mathbf{S}_{OMI_BC,i}^{-2} \quad (12).$$

3 where $\mathbf{T}_{OMI_BC_Flag}$ is the OMI AAOD flagged for the presence of carbonaceous
4 aerosols (which is different than Eq. 5 or 8 which depend upon prior model ratios). In
5 this case, the gradient of the cost function with respect to BC concentration at the
6 layer l will be

$$7 \quad \frac{\partial J}{\partial BC_l} = \frac{\partial \tau_{GC_BC,l,i}}{\partial BC_l} * (\mathbf{T}_{GC_BC,i} - \mathbf{T}_{OMI_BC_Flag,i}) * \mathbf{S}_{OMI_BC,i}^{-2} \quad (13).$$

8 The implications of the different cost function formulations will be described in
9 Section 4.1.

10 **3 Impacts of BC anthropogenic emission uncertainties**

11 In this section, we quantify the extent to which differences in anthropogenic emission
12 inventories contribute to uncertainties in simulated surface BC and AAOD. Here, the
13 SEAC⁴RS emission inventory is appended to the MEIC emission inventory outside of
14 China for the Southeast Asian nested simulation (MEIC_SEAC⁴RS). Figure 4 shows
15 the impact of different BC anthropogenic emission inventories on simulated surface
16 BC concentrations and comparisons to in situ measurements over China [Zhang et al.,
17 2008, Cao et al., 2009]. The monthly and daily ground-based measurements at sites
18 representative of four different regions are shown: northern China (Gucheng, GUC),
19 northeastern China (Longfengshan, LFS), southern China (Nanning, NAN), and
20 midwestern China (XiAn, XIA). Generally, the modeled and observed BC
21 concentrations are higher in winter than in summer. In addition to enhanced
22 anthropogenic emissions during the winter [Fu et al., 2012], the Asian summer

1 monsoon plays an important role in this seasonal cycle by reducing aerosol
2 concentrations in the summer over China [Zhang et al., 2010]. Though the model
3 simulation is able to capture the seasonal variability, it underestimates surface BC
4 concentration at the urban sites, such as GUC, NAN, and XIA, with all of these
5 anthropogenic emission inventories, except at NAN, where the SEAC⁴RS inventory
6 leads to values as high or higher than observed, but the seasonal variation has not yet
7 been reproduced. With the INTEX-B and MEICS inventory, though the surface BC
8 concentrations are underestimated at some background and rural sites [Fu et al., 2012;
9 Wang et al., 2013], the simulated BC surface concentrations at the rural site of LFS
10 are quite comparable to the observation, especially the seasonal variations. The
11 INTEX-B and MEIC inventories improve the BC concentrations in winter with the
12 inclusion of monthly variability over China compared to the inventories of Bond and
13 SEAC⁴RS.

14 The spatial distributions of simulated surface BC concentrations using
15 MEIC_SEAC⁴RS and INTEX-B inventories are compared to the in situ observation at
16 20 sites over Southeast Asia for April and October 2006 in Fig. 5. The east to west
17 gradient in China and the north to south gradient in India are not well reproduced by
18 the model, where the simulated BC concentrations are much lower over eastern China
19 and the IGP for both April and October, especially for the urban areas since the model
20 is unable to resolve individual urban hot spots [Fu et al., 2012].

21 Figure 6a shows the differences in monthly average AAOD between the model using
22 the MEIC_SEAC⁴RS inventory and OMI (former minus latter) for April and October

1 2006. GEOS-Chem underestimates AAOD compared to OMI across broad areas of
2 Southeast Asia in April, especially eastern China and the IGP. In October, AAOD is
3 underpredicted over northern China while it is over predicted over eastern China and
4 most of South Asia. Corresponding OMI data counts towards the monthly average at
5 each grid cell are shown in Fig. 6b. In general, more data are available over northern
6 China and India. We note that the data counts are much lower in October compared to
7 April over southern China and the Indo China Peninsular, where the observations are
8 overestimated. Sparse OMI observations over these areas may result in apparent high
9 or low biases. If we only take into account the OMI_AAOD_BC retrievals, the
10 differences and corresponding OMI data counts for April and October are shown in
11 Fig. 7. The spatial distributions are quite similar to those using all AAOD
12 observations shown in Fig. 6, but with much larger negative differences over Asia in
13 April and over northern China and IGP in October. The data counts are also smaller
14 when only considering the OMI_AAOD_BC observations, especially over the dust
15 source regions and downwind areas in April and broad areas over South Asia in
16 October.

17 We also compared the observed to simulated AAOD using different emission
18 inventories (figures not shown here). The simulated AAOD is comparable using
19 INTEX-B and MEIC emission inventories over eastern China, while it is much lower
20 than the OMI column retrieval using the inventories of Bond and SEAC⁴RS. With the
21 SEAC⁴RS inventories, the simulated AAOD over the IGP shows enhancements
22 compared to that using Bond and INTEX-B inventories.

1 **4. Uncertainties of observation and penalty terms**

2 **4.1 Adjoint forcing**

3 As described in Section 2.5, there are four methods to formulate the observation term
4 of the cost function owing to different approaches of deriving an “observed” BC
5 AAOD. We perform sensitivity experiments to quantify the impact of using these
6 different formulations. For these tests, only the observation term is considered in the
7 cost function (i.e., the penalty term is not included), and we use the same
8 anthropogenic emission inventory (MEIC_SEAC⁴RS) as the prior emissions for each
9 test. Figure 8 shows the results of the differences between optimized and prior
10 anthropogenic BC emissions based on the four approaches.

11 Qualitatively, there are many noticeable differences between the optimization results
12 using the different formulations of the observation operator. In April, enhanced
13 anthropogenic BC emissions are shown over broad areas using all four methods.
14 However, slight reductions appear over eastern China and southern India when using
15 method (b), (c) and (d). In particular, method (c) results in lower posterior emissions
16 over China. The results of methods (c) and (d) are quite consistent except the
17 enhancements of posterior emissions over southern India occur using method (d).
18 Similarly, although the four optimized patterns are quite consistent in October, much
19 larger areas of BC emissions reduction result from using method (c). The reductions
20 of method (d) are similar to that of method (c) over eastern China, while quite
21 different over India with significantly enhanced posterior emissions.

22 The differences in results are related to different assumptions implicit in the various

1 forms of the cost function considered. Both method (a) and method (b) depend on the
2 relative ratio of BC to other absorbing aerosol (e.g. dust, OC) in the model. Further,
3 method (a) introduces a stronger dependency on the GEOS-Chem prior vertical
4 distribution, since the observation operator includes three dimensions with all vertical
5 layers, compared to the column based method (b). Since there are more observations
6 over IGP and northeastern China in April, this stronger constraint may enhance the
7 negative forcing due to the model underestimation, which leads to increasing
8 emissions. Since, through the adjustment of the OMI data to generate the OMI_GC
9 product, we have already used the GEOS-Chem prior information on the aerosol
10 vertical distribution, it seems preferable to adopt a column-based approach for the
11 assimilation. Though both method (b) and method (c) are based on the column
12 AAOD, the former assumes that the relative contributions of BC to total AAOD in the
13 model is correct, while the latter assumes that absolute contributions of OC and dust
14 are correct. The simulated total AAOD might not be equivalent to the observed
15 AAOD after optimization in both method (a) and method (b) since the adjoint forcing
16 only accounts for the BC AAOD. In addition, the results would highly depend on the
17 model performance in simulating the ratio between BC and other absorbing aerosol.
18 There are no significant biases for the GEOS-Chem simulated fraction of coarse model
19 dust mass [Wang et al., 2012, Philip et al., 2014], which suggests that the simulated
20 dust AAOD fraction is likely unbiased. However the simulated mass of both BC and
21 OC in GEOS-Chem are biased low [Heald et al., 2005; Fu et al., 2012]. We thus
22 adopt method (c), since the strength of the adjoint forcing with respect to BC sources

1 depends upon the BC absolute contribution in AAOD rather than the relative
2 contribution of method (b), which may have less model dependency in simulating the
3 distribution of other aerosols. The major differences between method (c) and method
4 (d) are the available observation data counts, as the data counts of the latter are much
5 fewer than the former. In April, the pattern of optimized emissions using method (c)
6 and method (d) are quite consistent, suggesting that BC AAOD play a dominant role
7 in contributing to the total AAOD. We will adopt method (c) for the following
8 experiments and also discuss method (d) in section 5.4 for comparison.

9 **4.2 Penalty Term**

10 The inclusion of a penalty, or background term, in the cost function is a key factor for
11 inverse modeling. It is specified through the prior (background) error covariance
12 matrix, \mathbf{S}_a , and a regularization parameter γ_r . In the absence of rigorous statistical
13 information on the error covariance of the emissions, we assume the errors are
14 uncorrelated and use an L-curve selection criterion to identify an optimal value of γ_r
15 [Hansen, 1998; Henze et al., 2009]. The uncertainties of BC are assumed to be 100%
16 of the maximum BC emissions over the simulation domain. Thus, the optimal values
17 of γ_r are selected to be 0.5 for April and 1.0 for October based on the
18 MEIC_SEAC⁴RS emission and the cost function in Eq. (10). The contribution of the
19 penalty term results in smaller adjustments to emissions, as the regularized results
20 prefer smoother solutions than those of the unconstrained inversion tests in Fig. 8.
21 Here we assume a single constant value for \mathbf{S}_a along the diagonal and no off-diagonal
22 terms.

1

2 **5. Analysis of Optimizations**

3 We next proceed to constrain Southeast Asian BC sources using OMI AAOD. The
4 OMI AAOD observations are compared to model estimates from GEOS-Chem nested
5 simulation for April and October 2006 using the difference between simulated total
6 AAOD and observed OMI AAOD (i.e., Eq. (10)). Tens of thousands of OMI
7 retrievals per month are available for the assimilation, but not all of the retrievals are
8 usable. In the presence of cirrus clouds, retrievals errors are significant. The effect of
9 optically thin cirrus is similar to that of subpixel cloud contamination. As plumes of
10 dust or smoke aerosol drift away from their source regions, they become mixed with
11 clouds. This problem is particularly evident over the oceans, which are frequently
12 covered with thin cirrus and fair-weather cumulus clouds. Generally, the retrieved
13 AAOD shows a reduced coverage especially over the oceans due to cloud
14 contamination and the effects of sun glint [Torres et al., 2007]. Thus, quality and
15 diagnostic flags are defined to classify and filter the retrievals. In October, only
16 observations north of 5°N are included for data assimilation to minimize contributions
17 of biomass burning from Indonesian fires.

18 **5.1 Optimized emissions**

19 Considering the performances of the four emission inventories discussed in Section
20 2.3, the following optimized results will mainly focus on using the MEIC_SEAC⁴RS
21 and INTEX-B inventories. The prior and posterior (optimized) BC emissions from
22 anthropogenic sources are shown in Fig. 9. Overall, the results show an enhancement

1 in BC emissions over broad areas of Southeast Asia, with adjustments that are
2 seasonally and spatially heterogeneous. This is consistent with the top-down
3 constraints on BC emissions based on ground-base measurements by Fu et al., [2012],
4 which also show that the BC emissions are greatly enhanced across broad areas of
5 China, in particular northern and central China and the megacity clusters. In April,
6 either using MEIC_SEAC⁴RS or INTEX-B inventories, large increases of up to a
7 factor of 3-5 are shown after optimization. The largest enhancements occur sharply in
8 eastern China and the IGP in April by up to a factor of five (Fig. 9). Other large
9 increases are located in South Asia, northeastern and northwestern China. There is a
10 small decrease in anthropogenic BC in part of southwestern China. That is quite
11 different from the inversion results based on AOD by Xu et al. [2013], wherein the
12 optimized anthropogenic BC emissions are reduced by 9.1% over China, even though
13 the prior BC anthropogenic emissions that they used are from Bond et al., [2004,
14 2007], which much lower than what we used. The dust scheme had not yet been
15 updated and modified in Xu et al., [2013] following the revised particle size
16 distribution suggested in Zhang et al. [2013]. Thus it is possible that overestimated
17 dust and AOD projected a model bias onto adjustments of emissions of all type of
18 aerosols over dust regions and downwind areas, such as eastern China. However, the
19 adjustments of anthropogenic BC emissions before and after optimization in October
20 are different than those in April (Fig. 10). The optimization of anthropogenic
21 emissions yields a slight reduction (1~5%) over central India and part of southern
22 China and an increase by 10~50% over eastern and northern China, as well as

1 northwestern India.

2 Though the adjusted patterns of optimized BC emission are basically comparable by
3 using MEIC_SEAC⁴RS and INTEX-B inventories, significant differences are located
4 over India and eastern China (Fig. 11). We also note that the differences in the
5 optimized results are almost the same as those of the prior emissions between
6 MEIC_SEAC⁴RS and INTEX-B inventories. The ratio between their posterior
7 differences and prior differences (see Fig. 11, right column) shows that the
8 optimization increases their differences, relative to the prior, over broad areas over
9 China and India up to a factor of three in April, with only slight decreases over south
10 India. In October, optimization decreases the posterior differences between
11 MEIC_SEAC⁴RS and INTEX-B emission inventories relative to the prior by 10-20%
12 over southern and most of India. Areas where prior differences are increased/reduced
13 are consistent with the areas where the emissions increase/decrease after optimization
14 (see Fig. 10). This suggests that absolute errors in the prior emissions may be larger
15 than the relative prior uncertainty percentages considered here.

16 In addition to reducing the bias of the emissions, it is important to consider how much
17 the inversion has reduced uncertainty in the emissions. A new method based on the
18 Broyden-Fletcher-Goldfarb-Shanno (BFGS) algorithm is used to estimate the
19 posterior uncertainty [Bousserez et al., 2014]. The posterior error reductions are up to
20 30% and 15% in April and October over the IGP and eastern China, where the
21 anthropogenic emission enhancements were the largest (Figure 9 and 10). The prior
22 errors do not change across broad areas, where the changes of optimized emissions

1 are relatively smaller.

2 While the most substantial adjustments are made to anthropogenic emissions, biomass
3 burning emission are also adjusted. The most significant increases are over South
4 Asia and eastern Europe in April, especially, the indo-China peninsula and eastern
5 Russia (figures not shown). The optimized biomass burning emissions in October
6 have the largest enhancements are over south Borneo and Sumatra. Similar to the
7 optimized anthropogenic emission, there is also not much change for the optimized
8 biomass burning emission throughout India and and indo-China peninsula in October.
9 To examine the impacts of different prior anthropogenic inventories on optimized
10 biomass burning emissions, we consider the following ratios:

$$11 \quad \frac{\Delta MEIC_SEAC4RS_{GFED3} - \Delta MEIC_SEAC4RS_{GFED2}}{GFED3 - GFED2} \quad (14).$$

12 Eq. 14 shows how changes in anthropogenic emissions during the optimization
13 compare when using two different biomass burning inventories, relative to the
14 difference in these biomass burning inventories themselves. Large values of this ratio
15 indicate regions where our top-down constrains on anthropogenic emissions are more
16 sensitive to errors in the prior biomass burning inventories, such as over eastern China
17 and the southern IGP (Fig. 12).

18 **5.2 Optimized BC AAOD**

19 The largest uncertainty reductions are obtained over eastern China and the IGP, so
20 here we consider AAOD in these regions alone. Fig. 13 shows the observed and
21 simulated BC AAOD over eastern China (105°-125°E, 20°-45°N) before and after
22 optimization in green along with linear line slope equation and correlation R². Here

1 the observed BC AAOD is derived from the OMI AAOD and the prior ratio of
2 simulated BC AAOD versus total AAOD. The prior BC AAOD is misrepresented and
3 underestimated compared to observation over eastern China, especially in April. The
4 low biases of the prior slopes are improved after optimization in April and October by
5 132% and 11%, respectively. Similar to the optimized BC concentrations, the
6 improvements in October after optimization are less significant than in April. There
7 are only slight changes in correlation coefficients, which may due to the large number
8 of samples in both spatial and temporal dimensions across which variations are not in
9 the same directions. In the IGP area, which we define as (70°-90°E, 23°-32°N), the
10 low biases of prior BC AAOD are much larger than those in eastern China (Fig. 14).
11 The values of most observed BC AAOD are lower than 0.3 and the slopes are 0.22
12 and 0.28 in April and October. After optimization, the slope increase by 155% and the
13 correlation coefficients change from 0.2 to 0.25 in April. In October, there is a 32%
14 increase in slope and the correlation coefficient doubles but still remains small (from
15 0.06 to 0.12).

16 Though slopes improve after optimization for both eastern China and India, they still
17 show considerable lower biases. This results, in part, from constraints of the penalty
18 term. Additionally, we note that many prior AAOD values are very small and close to
19 zero. These are hard for the optimization routine to adjust significantly in the areas
20 where the values of prior emission are very small or close to zero. Since the
21 optimization scheme is based on the use of emissions scaling factors, large gradients
22 with respect to BC concentrations will result in small gradients with respect to

1 emissions scaling factors in locations with small emissions. To test how much this
 2 formulation restricts the inversion, a sensitivity experiment was performed assuming
 3 uniform prior emissions in all grid boxes. This facilitates adjustments to prior
 4 emissions throughout the domain, resulting in larger posterior AAOD after
 5 optimization. However, the resulting spatial distributions and gradients of
 6 anthropogenic emissions are not realistic (e.g., large emissions are not placed in
 7 known source areas). Alternatively, instead of adjusting emissions through application
 8 of scaling factors, σ , to the a priori emissions, the BC emissions themselves could be
 9 treated as the control variables in the cost function (Eq. 15). Another sensitivity
 10 experiment is performed for April 2006, inverting for the emissions themselves rather
 11 than the emissions scaling factors. Figure S2 in supplemental shows the total
 12 emissions (summed across sectors) after optimization using different inversion
 13 approaches. Fig. S2a is result based on the scaling factor as describe by Eq. 2 in
 14 Section 2.4 that the range of emissions are constructed using scaling factors as control
 15 variables to adjust the vector of model emissions. Fig. S2b shows the results when
 16 emissions are constrained directly as the control variables in the penalty term as:

$$17 \quad J = \frac{1}{2} \sum_{\mathbf{c} \in \Omega} (\mathbf{H}\mathbf{c} - \mathbf{c}_{obs})^T \mathbf{S}_{obs}^{-1} (\mathbf{H}\mathbf{c} - \mathbf{c}_{obs}) + \frac{1}{2} \gamma_r (\mathbf{E} - \mathbf{E}_a)^T \mathbf{S}_a^{-1} (\mathbf{E} - \mathbf{E}_a) \quad (15).$$

18 This formulation allows the inversion to place significant emissions in areas where
 19 the prior emissions are very small or close to zero. The optimized emissions over the
 20 larger prior source areas, such as northeastern China and the middle IGP, are smaller
 21 than when optimizing scaling factors. These sensitivity tests demonstrate the value of
 22 using the prior emissions inventories, either explicitly or implicitly through scaling

1 factors, in terms of constraining the magnitude of known sources, and the downside in
2 terms of the difficulty in introducing new sources through the inversion.

3 We also evaluate (Fig. 15) the prior and posterior simulated AAOD against the OMI
4 and AERONET daily average AAOD at 4 sites where there are available
5 measurements during the periods of April and October, 2006 (see the red sites in Fig.
6 2): Beijing (BJ) in China, Kanpur (KP) and Gandhi_College (GH) in India, and
7 Mukdahan (MD) in Thailand. The daily average GEOS-Chem model results and OMI
8 AAOD are sampled according to the AERONET observations at the locations of the 4
9 sites. At the Beijing site, the prior model AAOD estimates driven either by
10 MEIC_SEAC⁴RS or INTEX-B inventories are underestimated by a factor of ~2,
11 while the posterior AAOD are more comparable to the observations in April. In terms
12 of temporal variability, the model is able to capture some features of peaks after
13 optimization. At the two sites in India, only a few measurements are available in late
14 April, but the magnitudes are close to OMI observation. The optimized results using
15 the MEIC_SEAC⁴RS inventory shows great improvements compared to the prior
16 AAOD. However, the optimized AAOD using the INTEX-B inventory still shows
17 negative biases. The differences in optimized AAOD between using INTEX-B and
18 MEIC_SEAC⁴RS come from their prior differences in AAOD. This again
19 demonstrates that the posterior optimization results are not independent of the prior
20 emission inventories, consistent with the estimated reduction in posterior error shown
21 in Fig 10. At the site of Gandhi_College (GH) and Mukdahan (MK) there are large
22 differences between the OMI and AERONET AAODs; the magnitudes of the OMI

1 AAOs are much lower than those from AERONET, even close to zero on some
2 days. Koch et al. [2009] compared the AERONET and OMI retrievals of AAOD at
3 AERONET sites. The results showed that the two retrievals broadly agree with each
4 other, but that the OMI AAOD is much smaller over Asia. In our study, only a few
5 OMI AAOD pixels are available in Thailand site (MK) (Fig. 6); these limited and
6 sparse observations do not provide enough information to robustly constrain
7 emissions in this region.

8 **5.3 Optimized surface BC concentrations**

9 As mentioned before, the prior surface BC concentrations are underestimated in most
10 of the urban and rural sites over China. Figure 16 shows the spatial distribution of
11 optimized surface BC concentrations compared to in situ measurements at 20 sites in
12 Southeast Asia. The largest in situ BC concentrations observed over eastern China
13 and the IGP, which are densely populated, industrialized areas, are now reproduced
14 well by the optimized simulation. After optimization, the spatial gradients of the
15 observed BC concentrations are captured by the model: high in the east and low in the
16 west for China, and high in the north and low in the south for India. Using the
17 MEIC_SEAC⁴RS inventory for the prior emissions, the optimized spatial distributions
18 are better simulated than when than using the INTEX-B inventory. In particular, the
19 simulated BC concentrations are much closer to the observations over the IGP after
20 optimization. The scatter plots in Fig. 17 show the correlations of BC concentrations
21 from surface observations and GEOS-Chem before (blue) and after (red)
22 optimization. Initial negative biases are shown in both April and October. The linear

1 regression slope increases by more than a factor of four in April. However, the
2 modeled BC concentrations at most of the sites only slightly change after the
3 optimization in October, which result in a much smaller improvement in the
4 regression slope (21%). The correlation coefficients increase by 0.04 to 0.08 after
5 optimization, such small improvement may be owing to the sparse spatial
6 distributions of the observational sites.

7 More specific site-by-site comparisons between model and observations are shown in
8 Fig. 18. Although the optimized BC surface concentrations are enhanced in April,
9 overestimation occurs in some eastern sites over China. In October, the low biases are
10 corrected both in the urban sites and rural sites, especially the eastern rural sites in
11 China. However, there is a persistent negative bias in most sites after optimization in
12 October. Due to the very low prior emissions, the optimization has less impact on the
13 western sites over China. The GEOS-Chem prior simulation underestimates surface
14 BC concentrations in all the urban sites and coastal sites over India in April (Fig. 16).
15 While the optimization enhances the BC sources and surface concentration, it still
16 shows a negative bias in most of sites over India, especially the urban sites. The
17 smaller improvement in coastal sites is not only due to the low prior emissions but
18 also the large uncertainties of AAOD retrieval for low aerosol amounts over the
19 ocean.

20 Given the stark contrast between the inversion results in April and October, we also
21 conducted the optimization for two additional months in winter (January) and summer
22 (July) season using MEIC_SEAC⁴RS as the prior inventory. In January, the

1 anthropogenic emissions show enhancements over the IGP and parts of western and
2 northern China and slight decreases over southern India and eastern and southern
3 China (figures not shown here), which results in increasing the surface BC
4 concentrations in XIA and LFS sites while decreasing concentrations in the sites of
5 GUC and NAN (see Fig. 4). In July, there is no significantly change for the surface
6 BC concentrations after optimization owing to very sparse observation in July over
7 eastern China. From this seasonal comparison, it appears that the BC anthropogenic
8 emissions are not always underestimated during the year. The largest
9 underestimations across the whole region of Southeast Asia occur in April. The
10 underestimated regions are mainly over IGP and northern China in both January and
11 October. The slight overestimates are indicated over southern India and part of
12 eastern China in January as well as northern China in July.

13 Discrepancies versus surface observations might also relate to model representational
14 error incurred by comparing ~50 km gridded estimates to in situ BC measurements,
15 which likely have finer length-scales of variability [Wang et al., 2013; Cohen and
16 Prinn, 2011; Cohen et al., 2011]. Considering the coarse resolution of the model
17 when comprising with the ground-based measurements, we investigate the impacts of
18 model resolution by considering approaches for downscaling the model simulations.

19 One approach is to use high-resolution population datasets to redistribute primary
20 aerosol concentrations [e.g., Krol et al., 2005; UNEP, 2011; Silva et al., 2013]. Based
21 on a finer resolution population density dataset, a parameterization of the urban
22 increment for non-reactive primary emitted anthropogenic BC and organic matter has

1 been developed and tested for coarse resolution air quality model. This method does
2 not alter concentrations at rural sites since it assumes that results at coarse resolution
3 only represent the rural (background) sites. According to this method, we used a high-
4 resolution ($1/24^\circ \times 1/24^\circ$) population dataset of Gridded Population of the World,
5 Version 3 (GPWv3, [http://sedac.ciesin.columbia.edu/data/set/gpw-v3-population-](http://sedac.ciesin.columbia.edu/data/set/gpw-v3-population-density-future-estimates)
6 [density-future-estimates](http://sedac.ciesin.columbia.edu/data/set/gpw-v3-population-density-future-estimates)) to downscale and adjust the simulated BC concentration at
7 urban sites (defined locations where population density exceeding $600/\text{km}^2$). The
8 scatter plots (Fig. 17b) show that, on average, the application of population
9 downscaling improves the performance of the modeled results compared to the non-
10 adjusted BC concentrations in April for both the prior and posterior simulations,
11 although low biases remain in each. It does not make any change in the slope in
12 October after applying the population parameterization, and correlation is degraded.
13 Downscaled estimates at only two sites (LIA and NAN) show enhancements, the rest
14 are not impacted.

15 To more directly investigate the impact of model resolution, it would be ideal to
16 compare the results of the present simulations to higher resolution simulations with
17 the same model [e.g., Pungler and West, 2013]. While this is not currently an option
18 for this model version, we can conduct GEOS-Chem simulations at a coarser
19 resolution (2° latitude \times 2.5° longitude) and make inferences about the role of
20 resolution errors. Fig. 19 shows the resolution errors in estimated surface BC
21 concentrations in the coarse resolution results ($2^\circ \times 2.5^\circ$) with respect to fine
22 resolution simulations ($0.5^\circ \times 0.667^\circ$). The resolution error exceeds 20% across broad

1 areas, and even up to 300% over the IGP and part of Southeastern Asia. The surface
2 BC concentrations are much lower using coarse resolution over the major source
3 regions, in particular the IGP, where the resolution error is more than 3. This is likely
4 owing to coarse grid boxes not describing the sharp gradient between high
5 concentrations in the valley and low concentrations in the mountain. The optimized
6 surface BC concentrations from our $0.5^\circ \times 0.667^\circ$ simulations are underestimated by a
7 factor of 2-3 at the IGP sites compared to in situ measurements. Pungert and West
8 [2013] show that the percent difference between all-cause mortality estimates at 12
9 km resolution and at coarser resolutions of 36 km and 96 km for BC is ~9% and
10 ~23% respectively. Assuming that model skill at estimating variations in
11 concentrations at the scales of the in situ measurements is similar to that for
12 estimating exposure based on highly resolved populations distribution, we can
13 extrapolate from the results of Pungert and West [2013] that the resolution errors in the
14 $0.5^\circ \times 0.667^\circ$ simulation, relative to the scale of the measurements, is a bit less than the
15 resolution error in the $2^\circ \times 2.5^\circ$ simulation relative to the $0.5^\circ \times 0.667^\circ$ simulation
16 Thus, the former may be as large as a factor of ~2.5 in individual grid cells.

17 **5.4. Comparisons using OMI_AAOD_BC**

18 A subset of the OMI retrievals (OMI_AAOD_BC) represents the presence of
19 carbonaceous aerosols. Using only these retrievals for the inversion, the differences
20 between prior and posterior (later minus former) BC anthropogenic emissions using
21 MEIC_SEAC⁴RS inventory are shown in Fig. 20. Compared to Fig. 9 and Fig. 10,
22 there are similar signs of emissions adjustments over most of Southeast Asia except in

1 October over India where reductions are not shown in the posterior emissions due to
2 fewer available observations in the OMI_AAOD_BC data subset. Moreover, the
3 magnitudes of enhanced emissions in April are much larger if we use only the
4 OMI_AAOD_BC retrievals. This also results in larger posterior surface BC
5 concentrations (figures not shown) in some area and AAOD that improve the
6 underestimates in a few sites when compared to the ground-base measurements and
7 AERONET observation. However, the differences are not obvious in October and the
8 improvements in April are neither significant nor widespread. Considering there are
9 less observations available using OMI_AAOD_BC, especially in October and other
10 summer month (e.g. July), and that it does not change the major conclusions
11 compared to using OMI AAOD, using OMI AAOD is recommended.

12

13 **6. Summary and Discussions**

14 In this study, we used space-based observations of absorbing aerosol optical depth
15 (AAOD) from the OMI instrument to constrain BC monthly average emissions for
16 April and October, 2006, with the GEOS-Chem model and its adjoint. First, we
17 evaluated the model simulated BC concentrations using four different anthropogenic
18 emission inventories. The differences in these inventories exceeded 100% across
19 broad areas of Southeast Asia. For each of the four emission inventories, the
20 simulated surface BC concentrations had low biases compared to the available surface
21 observations in most urban sites in Southeast Asia.

22 The adjoint model was used to perform 4D-Var inverse modeling to constrain BC

1 emissions. After optimization, both anthropogenic and biomass burning emissions
2 were adjusted. Either using the MEIC_SEAC⁴RS or INTEX-B inventory, the
3 optimized anthropogenic emissions for BC were significantly enhanced over broad
4 areas of Southeast Asia in April compared to the prior emission, with the largest
5 enhancements in eastern China and India IGP of up to a factor of five. From analysis
6 of inversions using different prior biomass burning inventories it was shown that
7 optimized anthropogenic emissions was most sensitive to the prior biomass burning
8 over eastern China and southern IGP. The adjustments in October were smaller than
9 those in April. Inverse modeling in additional months indicated that BC
10 anthropogenic emissions were not always underestimated throughout the year. The
11 largest underestimates occurred in April throughout Southeast Asia. Only slight
12 overestimates were indicated over southern India and eastern China for both January
13 in July. Inversion results were in general similar using either all OMI AAOD or just
14 the OMI_AAOD_BC. In October, the posterior anthropogenic emissions yielded a
15 slight reduction (1~5%) over central India and part of southern China while they
16 increased by 10~50% over eastern and northern China, as well as northwestern India.
17 The uncertainty of the posterior emissions over the IGP and eastern China were
18 estimated to have reduced up to 30% and 15% in April and October.

19 After optimization, the low model biases for BC AAOD improved by 132% and 11%
20 over Southeast Asia in April and October, respectively. In eastern China, these
21 improvements were more significant (143% and 30% in April and October). The
22 remaining residual error in the simulated OMI AAOD, which was significant in

1 October, particularly in India, may be a consequence of the inverse modeling
2 framework, which had difficulty introducing emissions in locations where the prior
3 emissions were close to zero. This downside may be overcome by performing
4 inversions directly for the emissions, rather than emissions scaling factors.

5 Results of the inversion were also compared to remote and in situ measurements that
6 were not assimilated. The posterior AAOD were quite comparable to AERONET
7 AAOD observations in April in China; however, large discrepancies remained at the
8 sites over India and Thailand after data assimilation. These residual errors compared
9 to AERONET may be associated with the limited and sparse observations of OMI
10 AAOD in these regions, which themselves were not very consistent with the
11 AERONET AAOD. Low biases of surface BC concentrations were improved or
12 corrected at urban sites and eastern rural sites over China in April, with the linear
13 regression slope between model and observed values increasing by more than a factor
14 of four. However, the adjustments were not strong enough in most sites over India in
15 April and October and over China in October. Moreover, the optimization had less
16 impact on the western sites over China and coastal sites over India due to the very low
17 prior emissions and the large uncertainties in AAOD retrieval for low aerosol
18 amounts over ocean. Model resolution error was also an important factor contributing
19 to discrepancies of BC concentrations compared to in situ measurements. Comparison
20 to coarser model simulations and the results of Pungler and West [2013] indicates that
21 the resolution errors may be up to a factor of 2.5 in grid cells in regions such as the
22 IGP and part of southeastern Asia.

1 Overall, this work was the first attempt to formally use the absorbing aerosol products
2 from satellite observation for a BC emissions inversion. Both the simulated AAOD
3 and surface BC concentration showed significant improvements spatially and
4 temporally after data assimilation, especially in April. However, there were still
5 several sources of uncertainty and limitations of this work worth considering. Aspects
6 such as model error and assumptions made regarding the observations and
7 uncertainties in the observations and prior emissions inventories contributed greatly to
8 uncertainties in the optimization results.

9 Our estimate that the errors in the prior emissions were only 100% restricted the
10 magnitude of the emissions adjustments allowed by the inversion. One might
11 conclude that such restrictions were too strict; however, uncertainties in emissions
12 were also not likely the only source of the discrepancy between observed and
13 predicted BC concentrations and AAOD. Textor et al. [2007] noted that inter-model
14 differences were only partially explained by differences in emission inventories;
15 removal processes also play an important role in affecting the lifetime and
16 concentrations of BC in the free troposphere. Although the 1 day aging from
17 hydrophobic BC to hydrophilic BC in GEOS-Chem is typical for this type of model
18 [Koch et al., 2009], aerosol internal mixing that includes effects of various physical,
19 chemical, and meteorological processing can also significantly impact BC
20 concentrations and aerosol absorptions [Stier et al., 2006; Cohen and Prinn 2011;
21 Cohen et al., 2011; Buchard et al., 2014], in some cases even more so than
22 uncertainties in emissions [Shen et al., 2014]. The scheme used in our study for

1 aerosol scavenging was based on Liu et al., [2001], which did not distinguish between
2 rain and snow. The recent updates by Wang et al. [2011] included corrections to
3 below-cloud and in-cloud scavenging that improved the overestimation of integrated
4 scavenging [Dana and Hales, 1976]. Corresponding updates to the wet scavenging in
5 the GEOS-Chem adjoint might also be helpful for improving the optimized results.

6 The optimizations were sensitive to how model information was used to calculate BC
7 component of the measured AAOD, which alone provided only a constraint on the
8 column concentrations of all absorbing aerosol (i.e., including dust and OC). We
9 have adjusted the OMI AAOD by applying the GEOS-Chem simulated aerosol layer
10 height to reduce the differences in the vertical profiles between the model and
11 observation. However, there could be inconsistent treatment of microphysical and
12 optical properties used in the AAOD calculation between the model and OMI
13 retrievals. The results of the optimization may be biased by error in the model's
14 vertical distribution of BC, which has been adjusted in other studies [van Donkelaar et
15 al., 2013]. It is important to realize that BC from most emission sources contained
16 not only elemental and organic fractions [Chow et al., 2009], but also non-soot OC,
17 i.e., brown carbon, that has a significant absorbing component at short wavelengths
18 comparable to elemental carbon absorption [Jacobson, 1999; Kirchstetter et al., 2004;
19 Andreae and Gelencser, 2006; Hoffer et al., 2006; Magi et al., 2009]. However,
20 absorbing aerosols in GEOS-Chem only include BC, OC and dust, while the brown
21 carbon has not yet been taken into account. While the attribution of ambient aerosol
22 absorption to BC may be a reasonable approximation in areas dominated by fresh soot

1 emissions, it may lead to misleading estimates of the AAOD when other light absorbing
2 particles were present since the brown carbon contributed 28% on average of the total
3 absorption at the wavelength of 440 nm [Bahadur et al., 2012]. It undoubtedly resulted
4 in overestimation of BC emissions after optimization in the areas where brown carbon
5 and other absorbing aerosols were considered in the observed AAOD.

6 Lastly, it is well known that the quality of the observation data plays the most
7 important role in data assimilation. Although the OMI AAOD retrieval provided much
8 better spatial and temporal coverage than the remote sensing measurements, such as
9 AERONET, we noted that there were large discrepancies between OMI AAOD and
10 AERONET observation in some areas, especially in October (See Fig. 15). Normally,
11 the OMAERUV retrievals were more reliable over land than over water since the
12 ocean surface reflectance show distinct angular and spectral variations. The major
13 factor affecting the quality of the OMI aerosol product was sub-pixel cloud
14 contamination due to the relatively large footprint of the OMI observations [Torres et
15 al., 1998]. Satheesh et al. [2009] demonstrated the potential of multisatellite analysis
16 of A-train data to improve the accuracy of retrieved aerosol products and suggested
17 that a combined OMI-MODIS-CALIPSO retrieval had potential to further improve
18 assessments of aerosol absorption, which would possible enhance the observation
19 quality in data assimilation. Important algorithm improvements have been
20 implemented in the current OMAERUV algorithm and the carbonaceous aerosol
21 model was replaced with a new model that accounted for the presence of OC while
22 the previous aerosol model only assumed black carbon as the absorbing component

1 [Jethva and Torres, 2011]. Recently, other improvements included the development of
2 CALIOP-based aerosol layer height climatology and the use of AIRS carbon
3 monoxide real time observations to distinguish smoke from dust type aerosols, which
4 improved the retrieval performance by 5-20% [Torres et al., 2013]. Using the updated
5 OMAERUV when it becomes available will likely improve the optimization results in
6 future work.

7 **Acknowledgement.**

8 This work was supported from Environmental Protection Agency-STAR grant RD-
9 83503701-0. Although the research described in the article has been funded wholly or
10 in part by the U.S. EPA's STAR program through grant (RD-83503701-0), it has not
11 been subjected to any EPA review and therefore does not necessarily reflect the views
12 of the Agency, and no official endorsement should be inferred.

13

1 **Table captions.**

2 Table 1 Comparison of BC anthropogenic emissions over eastern China (105°-125°E,
3 20°-45°N) and IGP (70°-90°E, 23°-32°N), unit: Tg.

| Domain | Prior emissions (MEIC_SEAC4RS) | | Posterior emissions (with penalty term) | | Posterior emissions (without penalty term) | |
|------------------|-----------------------------------|---------|--|---------|---|---------|
| | April | October | April | October | April | October |
| Eastern China | 0.11 | 0.11 | 0.30 | 0.11 | 0.22 | 0.12 |
| IGP | 0.04 | 0.04 | 0.14 | 0.04 | 0.11 | 0.05 |

4

5 **Figure captions.**

6

7 **Figure 1.** Absolute and relative differences in AAOD between OMI_Final and
8 OMI_GC AAOD for April and October, 2006.

9

10 **Figure 2.** Twenty sites of ground measurements (black dots) and four sites of
11 AERONET observation (red cross dots). Also shown are terrain heights (color shaded
12 contours, unit: m).

13

14 **Figure 3.** Annual anthropogenic emission of BC regridded into GEOS-Chem
15 resolution of $0.5^\circ \times 0.667^\circ$ from the inventories of (a) Bond, (b) INTEX-B, (c)
16 SEAC4RS, and (d) MEIC.

17

18 **Figure 4.** Comparison of the observed and simulated surface BC concentrations using
19 four emission inventories at the site of GUC, LFS, NAN, XIA. The orange dots are
20 the monthly mean posterior surface BC concentrations at these sites using MEIC
21 inventory over China.

22

23 **Figure 5.** Spatial distributions of prior surface BC concentrations using INTEX-B and
24 MEIC_SEAC⁴RS inventories overlaid with BC in situ measurements of 20 sites.

25

26 **Figure 6.** (a) Differences of monthly average AAOD between model using
27 MEIC_SEAC4RS inventory and the OMI observation (former minus latter) and (b)
28 corresponding OMI monthly data in each grid cell for April and October, 2006.

29

30 **Figure 7.** The same as Figure 6, but for OMI_AAOD_BC.

31

32 **Figure 8.** Differences between optimized and prior anthropogenic BC emissions
33 based on four methods of adjoint forcing (a) vertically resolved BC AAOD base on

1 model, (b) column BC AAOD based on model, (c) total OMI AAOD and (d) column
2 OMI_AAOD_BC for April and October, 2006.

3

4 **Figure 9.** Anthropogenic BC emissions for April, 2006. The first column shows the
5 prior inventory, the second the optimized inventory, the third the differences between
6 the prior and optimization, and the last column the relative changes of posterior error,
7 based on the inventories of (a) INTEX-B and (b) MEIC_SEAC⁴RS.

8

9 **Figure 10.** The same as Figure 8, but for October 2006.

10

11 **Figure 11.** Differences of anthropogenic BC emissions between using the inventories
12 of MEIC_SEAC⁴RS and INTEX-B for April and October 2006. The left column
13 shows the prior inventory, the center the optimized inventory, and right column the
14 between their posterior differences and prior differences.

15

16 **Figure 12.** The sensitivities of optimized anthropogenic emission based on GFED2
17 and GFED3 relative to the differences between GFED2 and GFED3.

18

19 **Figure 13.** Comparison of BC AAOD over eastern China (105°-125°E, 20°-45°N)
20 from OMI measurements and GEOS-Chem before and after the assimilation for April
21 and October, 2006.

22

23 **Figure 14.** Comparison of BC AAOD over IGP (70°-90°E, 23°-32°N) from OMI
24 measurements and GEOS-Chem before and after the assimilation for April and
25 October, 2006.

26

27 **Figure 15.** Comparison of total daily AAOD from OMI, AERONET and GEOS-
28 Chem before and after the assimilation at the four AERONET sites for April and
29 October, 2006.

30

31 **Figure 16.** Spatial distributions of optimized surface BC concentrations using
32 INTEX-B and MEIC_SEAC⁴RS inventories overlaid with BC in situ measurements
33 of 20 sites.

34

35 **Figure 17.** Comparison of monthly surface BC concentration for April and October,
36 2006, from in situ measurements and GEOS-Chem before and after the assimilation
37 (a) without and (b) with population density downscaling.

38

39 **Figure 18.** Comparison of monthly surface BC concentration from in situ
40 measurements and GEOS-Chem over (a) China and (b) India before and after the
41 assimilation using the inventories of MEIC_SEAC⁴RS and INTEX-B for April and
42 October, 2006.

43

44 **Figure 19.** The resolution errors of surface BC between the simulations of coarse

1 resolution ($2^\circ \times 2.5^\circ$) and fine resolution ($0.5^\circ \times 0.667^\circ$).

2

3 **Figure 20.** The differences between the prior and posterior anthropogenic BC
4 emissions for April and October, 2006, using OMI_AAOD_BC as the observation.

5

6

References

- Ackerman, A. S., Toon, O. B., Stevens, D. E., Heymsfield, A. J., Ramanathan, V., and Welton, E. J.: Reduction of tropical cloudiness by soot, *Science*, 288(5468), 1042–1047, doi:10.1126/science.288.5468.1042, 2000.
- Andreae, M. O. and Gelencsér, A.: Black carbon or brown carbon? The nature of light-absorbing carbonaceous aerosols, *Atmos. Chem. Phys.*, 6, 3131–3148, doi:10.5194/acp-6-3131-2006, 2006.
- Bahadur, R., Praveen, P. S., Xu, Y., and Ramanathan, V.: Solar absorption by elemental and brown carbon determined from spectral observations, *P. Natl. Acad. Sci. USA*, 109, 17366–17371, doi:10.1073/pnas.1205910109, 2012.
- Beegum, S. N., Moorthy, K. K., Babu, S. S., Satheesh, S.K., Vinoj, V., Badarinath, K.V.S., Safai, P.D., Devara, P.C.S., Singh, S., Vinod, Dumka, U.C., Pant, P.: Spatial distribution of aerosol black carbon over India during pre-monsoon season, *Atmos. Environ.*, 43(5), 2009, 1071–1078, 2009.
- Bey, I., Jacob, D. J., Yantosca, R. M., Logan, A. J., Field, B., Fiore, A. M., Li, Q., Liu, H., Mickley, L. J., and Schultz, M.: Global modeling of tropospheric chemistry with assimilated meteorology: Model description and evaluation, *J. Geophys. Res.*, 106, 23,073–23,095, 2001
- Bond, T. C. and Bergstrom, R. W.: Light absorption by carbonaceous particles: An investigative review, *Aerosol Sci. Tech.*, 40, 27–67, 2006.
- Bond, T. C., Bhardwaj, E., Dong, R., Jogani, R., Jung, S. K., Roden, C., Streets, D. G., and Trautmann, N. M.: Historical emissions of black and organic carbon aerosol from energy-related combustion, 1850–2000, *Glob. Biogeochem. Cy.*, 21, Gb2018, doi:10.1029/2006GB002840, 2007
- Bond, T. C., Doherty, S. J., Fahey, D. W., Forster, P. M., Berntsen, T., DeAngelo, B. J., Flanner, M. G., Ghan, S., Kärcher, B., Koch, D., Kinne, S., Kondo, Y., Quinn, P. K., Sarofim, M. C., Schultz, M. G., Schulz, M., Venkataraman, C., Zhang, H., Zhang, S., Bellouin, N., Guttikunda, S. K., Hopke, P. K., Jacobson, M. Z., Kaiser, J. W., Klimont, Z., Lohmann, U., Schwarz, J. P., Shindell, D., Storelvmo, T., Warren, S. G., and Zender, C. S.: Bounding the role of black carbon in the climate system: A scientific assessment, *J. Geophys. Res.*, 118, 5380–5552, doi: 10.1002/jgrd.50171, 2013.
- Bond, T. C., Streets, D. G., Yarber, K. F., Nelson, S. M., Woo, J. H., and Klimont, Z.: A technology-based global inventory of black and organic carbon emissions from combustion, *J. Geophys. Res.-Atmos.*, 109, D14203, doi:10.1029/2003JD003697, 2004.
- Bousserez, N., Henze, K. D., Perkins, A., Bowman, W. K., Lee, M., Liu, J., Deng, F., Jones, B. A. D.: Improved analysis error covariance matrix for high-dimensional variational inversions: application to source estimation using a 3D atmospheric transport model, *Q. J. R. Meteorol. Soc.*, submitted, 2014
- Buchard, V., M. da Silva, A., R. Colarco, P., Darmenov, A., A. Randles, C., Govindaraju, R., Torres, O., Campbell, J., and Spurr, R.: Using the OMI Aerosol Index and Absorption Aerosol Optical Depth to evaluate the NASA MERRA

- 1 Aerosol Reanalysis, *Atmos. Chem. Phys. Discuss.*, 14, 32177-32231,
2 doi:10.5194/acpd-14-32177-2014, 2014.
- 3 Byrd, R. H., Lu, H. P., Nocedal, J., and Zhu, C. Y.: A limited memory algorithm for
4 bound constrained optimization, *SIAM J. Sci. Comput.*, 16(5), 1190–1208, 1995
- 5 Cao, J. J., Lee, S. C., Chow, J. C., Watson, J. G., Ho, K. F., Zhang, R. J., Jin, Z. D., □
6 Shen, Z. X., Chen, G. C., Kang, Y. M., Zou, S. C., Zhang, L. Z., Qi, S. H., Dai,
7 M. H., Cheng, Y., and Hu, K.: Spatial and seasonal distributions of carbonaceous
8 aerosols over China, *J. Geophys. Res.*, 112, D22S11, doi:10.1029/2006JD008205,
9 2007.
- 10 Cao, J. J., Zhu, C. S., Chow, J. C., Watson, J. G., Han, Y. M., Wang, G., Shen, Z., and
11 An, Z. S.: Black carbon relationships with emissions and meteorology in Xi'an,
12 China, *Atmos. Res.*, 94,194–202, 2009
- 13 Charlson, R. J., and Pilat, M. J.: Climate: The influence of aerosols, *J. Appl. Met.*,
14 8(5), 1001–1002,1969
- 15 Chen, D., Wang, Y., McElroy, M. B., He, K., Yantosca, R. M., and Le Sager, P.:
16 Regional CO pollution and export in China simulated by the high-resolution
17 nested-grid GEOS-Chem model, *Atmos. Chem. Phys.*, 9, 3825–3839,
18 doi:10.5194/acp-9-3825-2009, 2009
- 19 Chin, M., Ginoux, P., Kinne, S., Torres, O., Holben, B. N., Duncan, B. N., Martin, R.
20 V., Logan, J. A., Higurashi, A., and Nakajima, T.: Tropospheric aerosol optical
21 thickness from the GOCART model and comparisons with satellite and sun
22 photometer measurements, *J. Atmos. Sci.*, 59, 461–483, 2002.
- 23 Chow, J. C., Watson, G. J., Doraiswamy, P., Chen, W. A., L., Sodeman, A. D.,
24 Lowenthal, H. D., Park, K., Arnott, P. W., and Motallebi, N.: Aerosol light
25 absorption, black carbon, and elemental carbon at the Fresno Supersite,
26 California, *Atmos. Res.*, 93(4), 874-887, 2009
- 27 Cohen, J. B. and Prinn, R. G.: Development of a fast, urban chemistry metamodel for
28 inclusion in global models, *Atmos. Chem. Phys.*, 11, 7629-7656,
29 doi:10.5194/acp-11-7629-2011, 2011.
- 30 Cohen, J. B., Prinn, R. G., and Wang, C.: The impact of detailed urban-scale
31 processing on the composition, distribution, and radiative forcing of
32 anthropogenic aerosols, *Geophys. Res. Lett.*, 38, L10808,
33 doi:10.1029/2011GL047417, 2011.
- 34 Cohen, J. B. and Wang, C.: Estimating Global Black Carbon Emissions Using a Top-
35 Down Kalman Filter Approach, *J. Geophys. Res. Atmos.*, 119, 307–
36 323doi: 10.1002/2013JD019912, 2014.
- 37 Cohen, J. B.; Quantifying the occurrence and magnitude of the Southeast Asian fire,
38 *Environ. Res. Lett.* 9, 114018 (13pp) 2014
- 39 Cooke, W. F., Liousse, C., Cachier, H., and Feichter, J.: Construction of a 1°x1° fossil
40 fuel emission data set for carbonaceous aerosol and implementation and
41 radiative impact in the ECHAM4 model, *J. Geophys. Res.*, 104, 22137–22162,
42 1999.
- 43 Cozic, J., Verheggen, B., Mertes, S., Connolly, P., Bower, K., Petzold, A.,
44 Baltensperger, U., and Weingartner, E.: Scavenging of black carbon in mixed

- 1 phase clouds at the high alpine site Jungfraujoch, *Atmos. Chem. Phys.*, 7, 1797–
2 1807, 2007
- 3 Dana, M. T. and Hales, J. M.: Statistical aspects of washout of polydisperse aerosols,
4 *Atmos. Environ.*, 10, 45–50, 1976
- 5 Dubovik, O. and King, D. M.: A flexible inversion algorithm for retrieval of aerosol
6 optical properties from Sun and sky radiance measurements, *J. Geophys. Res.*,
7 105, 20,673–20,696, 2000.
- 8 Dubovik, O., Holben, B. N., Eck, T. F., Smirnov, A., Kaufman, Y. J., King, M. D.,
9 Tanré, D., and Slutsker, I.: Variability of absorption and optical properties of key
10 aerosol types observed in worldwide locations, *J. Atmos. Sci.*, 59, 590–608,
11 2002a.
- 12 Dubovik, O., Holben, B. N., Lapyonok, T., Sinyuk, A., Mishchenko, M. I., Yang P.,
13 and Slutsker, I.: Non-spherical aerosol retrieval method employing light
14 scattering by spheroids, *Geophys. Res. Lett.*, 29(10),10.1029/2001GL014506,
15 2002b.
- 16 Dubovik, O., Sinyuk, A., Lapyonok, T., Holben, B.N., Mishchenko, M., Yang, P., Eck,
17 T.F., Volten, H., Muñoz, O., Veihelmann, B., van der Zande, W.J., Leon, J.-F.,
18 Sorokin, M., and Slutsker, I.: Application of spheroid models to account for
19 aerosol particle nonsphericity in remote sensing of desert dust. *J. Geophys. Res.*,
20 111, D11208, doi:10.1029/2005JD006619, 2006.
- 21 Dubovik, O., Smirnov, A., Holben, B.N., King, M.D., Kaufman, Y. J., Eck, T.F., and
22 Slutsker, I.: Accuracy assessment of aerosol optical properties retrieval from
23 AERONET sun and sky radiance measurements, *J. Geophys. Res.* ,105, 9791–
24 9806, 2000.
- 25 Eck, T. F., Holben, B. N., Reid, J. S., Dubovik, O., Smirnov, A., O’Neill, N. T.,
26 Slutsker, I., and Kinne, S.: Wavelength dependence of the optical depth of
27 biomass burning, urban, and desert dust aerosols, *J. Geophys. Res.*, 104(D24),
28 31,333–31,349, 1999
- 29 Fairlie, T. D., Jacob, J. D., Dibb, E. J., Alexander, B., Avery, A. M., van Donkelaar, A.,
30 and Zhang, L.: Impact of mineral dust on nitrate, sulfate, and ozone in
31 transpacific Asian pollution plumes, *Atmos. Chem. Phys.*, 10, 3999–4012,
32 doi:10.5194/acp-10-3999-2010, 2010.
- 33 Flanner, M. G., Zender, C. S., Randerson, J. T., and Rasch, P. J.: Present-day climate
34 forcing and response from black carbon in snow, *Geophys. Res.-Atmos.*, 112,
35 D11202, 10.1029/2006jd008003, 2007
- 36 Forster, P., Ramawamy, V., Artaxo, P., Berntsen, T., Betts, R., Fahey, D., Haywood, J.,
37 Lean, J., Lowe, D., Myhre, G., Nganga, J., Prinn, R., Raga, G., Schulz, M., and
38 Dorland, V. R.: Changes in Atmospheric Constituents and in Radiative Forcing,
39 in: *Climate Change 2007: The Physical Science Basis. Contributions of working
40 group I to the fourth Assessment Report on the Intergovernmental Panel on
41 Climate Change*, edited by Solomon, S., Wuin, D., Manning, M., Chen, A.,
42 Marquis, M., Averyt, K., Tignor, M., and Miller, H., Cambridge University
43 Press, Cambridge, United Kingdom and New York, NY, USA, 2007
- 44 Fu, T.-M., Cao, J. J., Zhang, X. Y., Lee, S. C., Zhang, Q., Han, Y. M., Qu, W. J.,

- 1 Han, Z., Zhang, R., Wang, Y. X., Chen, D., and Henze, D. K.: Carbonaceous
2 aerosols in China: top-down constraints on primary sources and estimation of
3 secondary contribution, *Atmos. Chem. Phys.*, 12, 2725-2746, doi:10.5194/acp-
4 12-2725-2012, 2012.
- 5 Giglio, L., Randerson, J. T., van der Werf, G. R., Kasibhatla, P. S., Collatz, G. J.,
6 Morton, D. C., and DeFries, R. S.: Assessing variability and long-term trends in
7 burned area by merging multiple satellite fire products, *Biogeosciences*, 7, 1171-
8 1186, 2010.
- 9 Giglio, L., van der Werf, G. R., Randerson, J. T., Collatz, G. J., and Kasibhatla, P.:
10 Global estimation of burned area using MODIS active fire observations, *Atmos.*
11 *Chem. Phys.*, 6, 957-974, doi:10.5194/acp-6-957-2006, 2006.
- 12 Ginoux, P., Prospero, M. J., Torres, O., and Chin, M.: Long-term simulation of global
13 dust distribution with the GOCART model: correlation with North Atlantic
14 oscillation. *Environ. Modell. and Softw.*, 19, 113-128, 2004.
- 15 Hakami, A., Henze, K. D., Seinfeld, H. J., Chai, T., Tang, Y., Carmichael, R. G., and
16 Sandu, A.: Adjoint inverse modeling of black carbon during the Asian Pacific
17 Regional Aerosol Characterization Experiment, *J. Geophys. Res.*, 110, D14301,
18 doi:10.1029/2004JD005671, 2005.
- 19 Hansen, A. D. A., Rosen, H., and Novakov, T.: The Aethalometer—An Instrument for
20 the Real-Time Measurement of Optical Absorption by Aerosol Particles, *Sci.*
21 *Total Environ.* 36:191-196, 1984.
- 22 Hansen, J., Sato, M., Ruedy, R., Lacis, A., and Oinas, V.: Global warming in the
23 twenty-first century: An alternative scenario, *P. Natl. Acad. Sci. USA*, 97(18),
24 9875-9880, 2000.
- 25 Hansen, J., and Nazarenko, L.: Soot climate forcing via snow and ice albedos, *Proc.*
26 *Natl. Acad. Sci.* 101(2), 423-428, doi:10.1073/pnas.2237157100, 2004. Hansen,
27 J., Sato, M., Ruedy, R., Nazarenko, L., Lacis, A., Schmidt, G. A., Russell, G.,
28 Aleinov, I., Bauer, M., Bauer, S., Bell, N., Cairns, B., Canuto, V., Chandler, M.,
29 Cheng, Y., Del Genio, A., Faluvegi, G., Fleming, E., Friend, A., Hall, T.,
30 Jackman, C., Kelley, M., Kiang, N., Koch, D., Lean, J., Lerner, J., Lo, K.,
31 Menon, S., Miller, R., Minnis, P., Novakov, T., Oinas, V., Perlwitz, Ja., Perlwitz,
32 Ju., Rind, D., Romanou, A., Shindell, D., Stone, P., Sun, S., Tausnev, N.,
33 Thresher, D., Wielicki, B., Wong, T., Yao, M., and Zhang, S.: Efficacy of climate
34 forcings, *J. Geophys. Res.*, 110, D18104, doi: 10.1029/2005JD005776, 2005.
- 35 Hansen, P. C.: Rank-Deficient and Discrete Ill-Posed Problems: Numerical Aspects of
36 Linear Inversion, SIAM, Philadelphia, USA, 1998.
- 37 Heald, C. L., Jacob, J. D., Park, J. R., Russell, M. L., Huebert, J. B., Seinfeld, H. J.,
38 Liao, H., and Weber, J. R.: A large organic aerosol source in the free
39 troposphere missing from current models, *Geophys. Res. Lett.*, 32, L18809,
40 doi:10.1029/2005GL023831, 2005.
- 41 Henze, D. K., Hakami, A., and Seinfeld, H. J.: Development of the adjoint of GEOS-
42 Chem, *Atmos. Chem. Phys.*, 7, 2413-2433, 2007.
- 43 Henze, D. K., Seinfeld, J. H., and Shindell, D. T.: Inverse modeling and mapping US
44 air quality influences of inorganic PM_{2.5} precursor emissions using the adjoint

- 1 of GEOS-Chem, *Atmos. Chem. Phys.*, 9, 5877–5903, doi: 10.5194/acp-9-5877-
2 2009, 2009.
- 3 Hoffer, A., Gelencser, A., Guyon, Kiss, P., G., Schmid, O., Frank, P. G., Artaxo, P.,
4 and Andreae, O. M.: Optical properties of humic-like substances (HULIS) in
5 biomass-burning aerosols, *Atmos. Chem. Phys.*, 6, 3563-3570, 2006.
- 6 Holben, B. N., Eck, F. T., Slutsker, I., Tanré, D., Buis, P. J., Setzer, A., Vermote, E.,
7 Reagan, A. J., Kaufman, J. Y., Nakajima, T., Lavenu, F., Jankowiak, I., Smirnov,
8 A.: AERONET--A federated instrument network and data archive for aerosol
9 characterization, *Remote Sens. Environ.*, 66, 1-16, 1998.
- 10 Hu, Y., Napelenok, L. S., Odman, T. M., and Russell, G. A.: Sensitivity of inverse
11 estimation of 2004 elemental carbon emissions inventory in the United States to
12 the choice of observational networks, *Geophys. Res. Lett.*, 36, L15806,
13 doi:10.1029/2009GL039655, 2009a
- 14 Hu, Y., Odman, T. M., and Russell, G. A., Top-down analysis of the elemental carbon
15 emissions inventory in the United States by inverse modeling using Community
16 Multiscale Air Quality model with decoupled direct method (CMAQ-DDM), *J.*
17 *Geophys. Res.*, 114, D24302, doi:10.1029/2009JD011987, 2009b
- 18 Huneus, N., Boucher, O., and Chevallier, F.: Atmospheric inversion of SO₂ and
19 primary aerosol emissions for the year 2010, *Atmos. Chem. Phys.*, 13, 6555-
20 6573, doi:10.5194/acp-13-6555-2013, 2013.
- 21 Jacobson, M. Z.: A physically-based treatment of elemental carbon optics:
22 Implications for global direct forcing of aerosols, *Geophys. Res. Lett.*, 27(2),
23 217–220, doi:10.1029/1999GL010968, 2000.
- 24 Jacobson, M. Z.: Isolating nitrated and aromatic aerosols and nitrated aromatic gases
25 as sources of ultraviolet light absorption, *J. Geophys. Res.-Atmos.*, 104(D3),
26 3527-3542, 1999
- 27 Janssen N.A., Hoek G., Simic-Lawson M., Fischer P., van Bree L., ten Brink H.,
28 Keuken, M; Atkinson, R. W., Anderson, H. R., Brunekreef, B., Cassee, F. R.:
29 Black Carbon as an Additional Indicator of the Adverse Health Effects of
30 Airborne Particles Compared with PM₁₀ and PM_{2.5}. *Environ Health Perspect*
31 119:1691-1699, 2011.
- 32 Janssen NAH, Lanki, T., Hoek, G., Vallius, M., de Hartog, J. J., Van Grieken, R.,
33 Pekkanen, J., Brunekreef, B.: Associations between ambient, personal and
34 indoor exposure to fine particulate matter constituents in Dutch and Finnish
35 panels of cardiovascular patients. *Occup. Environ. Med.*, 62:868–877, 2005
- 36 Jethva, H. and Torres, O.: Satellite-based evidence of wavelengthdependent aerosol
37 absorption in biomass burning smoke inferred from Ozone Monitoring
38 Instrument, *Atmos. Chem. Phys.*, 11, 10541–10551, doi:10.5194/acp-11-10541-
39 2011, 2011.
- 40 Jiang, Z., Jones, B. A. D., Kopacz, M., Liu, J., Henze, K., D., and Heald, C.:
41 Quantifying the impact of model errors on top-down estimates of carbon
42 monoxide emissions using satellite observations, *J. Geophys. Res.*, 116,
43 D15306, doi:10.1029/2010JD015282, 2011.
- 44 Johnson, B. T., Shine, P. K., and Forster, M. P.: The semi-direct aerosol effect: Impact

- 1 of absorbing aerosols on marine stratocumulus, *Quart. J. Roy. Meteor. Soc.*,
2 130(599), 1407–1422, doi:10.1256/qj.03.61, 2004.
- 3 Kirchstetter, T. W., Novakov, T., and Hobbs, V. P.: Evidence that the spectral
4 dependence of light absorption by aerosols is affected by organic carbon, *J.*
5 *Geophys. Res.-Atmos.*, 109, D21208, doi:10.1029/2004JD004999.12, 2004.
- 6 Koch, D., Schulz, M., Kinne, S., McNaughton, C., Spackman, J. R., Balkanski, Y.,
7 Bauer, S., Berntsen, T., Bond, T. C., Boucher, O., Chin, M., Clarke, A.,
8 De Luca, N., Dentener, F., Diehl, T., Dubovik, O., Easter, R., Fahey, D. W.,
9 Feichter, J., Fillmore, D., Freitag, S., Ghan, S., Ginoux, P., Gong, S.,
10 Horowitz, L., Iversen, T., Kirkevåg, A., Klimont, Z., Kondo, Y., Krol, M.,
11 Liu, X., Miller, R., Montanaro, V., Moteki, N., Myhre, G., Penner, J. E.,
12 Perlwitz, J., Pitari, G., Reddy, S., Sahu, L., Sakamoto, H., Schuster, G.,
13 Schwarz, J. P., Seland, Ø., Stier, P., Takegawa, N., Takemura, T., Textor, C.,
14 van Aardenne, J. A., and Zhao, Y.: Evaluation of black carbon estimations in
15 global aerosol models, *Atmos. Chem. Phys.*, 9, 9001-9026, doi:10.5194/acp-9-
16 9001-2009, 2009.
- 17 Kok, J. F.: A scaling theory for the size distribution of emitted dust aerosols suggests
18 climate models underestimate the size of the global dust cycle, *P. Natl. Acad.*
19 *Sci.*, 108(3), 1016-1021, 2011
- 20 Kondo, Y., Oshima, N., Kajino, M., Mikami, R., Moteki, N., Takegawa, N., Verma, L.
21 R., Kajii, Y., Kato, S., and Takami, A.: Emissions of black carbon in East Asia
22 estimated from observations at a remote site in the East China Sea, *J. Geophys.*
23 *Res.*, 116, D16201, doi:10.1029/2011JD015637, 2011
- 24 Kopacz, M., Jacob, D. J., Fisher, J. A., Logan, J. A., Zhang, L., Megretskaya, I. A.,
25 Yantosca, R. M., Singh, K., Henze, D. K., Burrows, J. P., Buchwitz, M.,
26 Khlystova, I., McMillan, W. W., Gille, J. C., Edwards, D. P., Eldering, A.,
27 Thouret, V., and Nedelec, P.: Global estimates of CO sources with high
28 resolution by adjoint inversion of multiple satellite datasets (MOPITT, AIRS,
29 SCIAMACHY, TES), *Atmos. Chem. Phys.*, 10, 855-876, doi:10.5194/acp-10-
30 855-2010, 2010.
- 31 Kopacz, M., Jacob, J. D., Henze, K. D., Heald, L. C., Streets, G. D., and Zhang, Q.: A
32 comparison of analytical and adjoint Bayesian inversion methods for
33 constraining Asian sources of CO using satellite (MOPITT) measurements of
34 CO columns, *J. Geophys. Res.*, 114, D04305, doi:10.1029/2007JD009264,
35 2009.
- 36 Kopacz, M., Mauzerall, D. L., Wang, J., Leibensperger, E. M., Henze, D. K., and
37 Singh, K.: Origin and radiative forcing of black carbon transported to the
38 Himalayas and Tibetan Plateau, *Atmos. Chem. Phys.*, 11, 2837-2852,
39 doi:10.5194/acp-11-2837-2011, 2011.
- 40 Krol, M., Houweling, S., Bregman, B., van den Broek, M., Segers, A.,
41 van Velthoven, P., Peters, W., Dentener, F., and Bergamaschi, P.: The two-way
42 nested global chemistry-transport zoom model TM5: algorithm and applications,
43 *Atmos. Chem. Phys.*, 5, 417-432, doi:10.5194/acp-5-417-2005, 2005.
- 44 Ku, B., and Park, J. R.: Inverse modeling analysis of soil dust sources over East Asia,

- 1 Atmos. Environ., 45(32), 5903–5912, doi:10.1016/j.atmosenv.2011.06.078,
2 2011
- 3 Levelt, P. F., Hilsenrath, E., Leppelmeier, G. W., van den Oord, G. H. J., Bhartia, P.
4 K., Tamminen, J., de Haan, J. F., Veefkind, J. P.: Science objectives of the
5 Ozone Monitoring Instrument, *IEEE Trans. Geosci. Remote Sens.*, 44(5), 1199-
6 1208, doi:10.1109/TGRS.2006.872336, 2006b.
- 7 Levelt, P. F., van den Oord, G. H. J., Dobber, M. R., Mälkki, A., Visser, H., de Vries,
8 J., Stammes, P., Lundell, J. O. V., Saari, H.: The Ozone Monitoring Instrument,
9 *IEEE Trans. Geosci. Remote Sens.*, 44(5), 1093-1101,
10 doi:10.1109/TGRS.2006.872333, 2006a.
- 11 Li, Y., Henze, K. D., Jack, D., Henderson, B., and Kinney, P.: Assessing public health
12 burden associated with exposure to ambient black carbon in the United States,
13 Under review by *Risk Analysis.*, 2014.
- 14 Lions, J. L.: *Optimal Control of Systems Governed by Partial Differential Equations*;
15 Springer-Verlag: Berlin, 1971.
- 16 Liu, H. Y., Jacob, J. D., Bey, I., and Yantosca, M. R.: Constraints from Pb-210 and Be-
17 7 on wet deposition and transport in a global three-dimensional chemical tracer
18 model driven by assimilated meteorological fields, *J. Geophys. Res. Atmos.*,
19 106, 12109–12128, 2001.
- 20 Liu, X. H., Penner, E. J., and Wang M. H.: Influence of anthropogenic sulfate and
21 black carbon on upper tropospheric clouds in the NCAR CAM3 model coupled
22 to the IMPACT global aerosol model, *J. Geophys. Res.*, 114, D03204,
23 doi:10.1029/2008JD010492, 2009.
- 24 Lu, Z., Zhang, Q., and Streets, D. G.: Sulfur dioxide and primary carbonaceous
25 aerosol emissions in China and India, 1996–2010, *Atmos. Chem. Phys.*, 11,
26 9839-9864, doi:10.5194/acp-11-9839-2011, 2011.
- 27 Luo, M., Rinsland, C. P., Logan, J. A., Worden, J., Kulawik, S., Eldering, A.,
28 Goldman, A., Shephard, M. W., Gunson, M., Lampel M.: Comparison of carbon
29 monoxide measurements by TES and MOPITT: The influence of a priori data
30 and instrument characteristics on nadir atmospheric species retrievals, *J.*
31 *Geophys. Res.*, 112, D09303, doi:10.1029/2006JD007663, 2007.
- 32 Ma, X., Yu, F., and Luo, G.: Aerosol direct radiative forcing based on GEOS-Chem-
33 APM and uncertainties, *Atmos. Chem. Phys.*, 12, 5563-5581, doi:10.5194/acp-
34 12-5563-2012, 2012.
- 35 Magi, B. I., Ginoux, P., Ming, Y., and Ramaswamy, V.: Evaluation of tropical and
36 extratropical Southern Hemisphere African aerosol properties simulated by a
37 climate model, *J. Geophys. Res.-Atmos.*, 114, D14204,
38 doi:10.1029/2008JD011128, 2009.
- 39 Martin, R. V., Jacob, D. J., Yantosca, R. M., Chin, M., and Ginoux, P.: Global and
40 regional decreases in tropospheric oxidants from photochemical effects of
41 aerosols, *J. Geophys. Res.*, 108, 4097, doi:10.1029/2002JD002622, 2003.
- 42 Moorthy, K. K., Beegum, S. N., Srivastava, N., Satheesh, S.K., Chin, M., Blond, N.,
43 Babu, S. S., Singh, S.: Performance evaluation of chemistry transport models
44 over India, *Atmos. Environ.*, 71, 210-225, 2013.

- 1 Omar, A. H., Winker, D. M., Tackett, J. L., Giles, D. M., Kar, J., Liu, Z., Vaughan, M.
2 A., Powell, K. A., and Trepte, C. R.: CALIOP and AERONET aerosol optical
3 depth comparisons: One size fits none, *J. Geophys. Res. Atmos.*, 118, 4748–
4 4766, doi:10.1002/jgrd.50330, 2013.
- 5 Oshima, N., Koike, M., Zhang, Y., Kondo, Y., Moteki, N., Takegawa, N., and
6 Miyazaki, Y.: Aging of black carbon in outflow from anthropo-genic sources
7 using a mixing state resolved model: Model development and evaluation, *J.*
8 *Geophys. Res.*, 114, D06210, doi:10.1029/2008JD010680, 2009.
- 9 Park, R. J., Jacob, J. D., Chin, M., and Martin, R. V.: Sources of carbonaceous
10 aerosols over the United States and implications for natural visibility, *J. Geophys.*
11 *Res.*, 108(D12), 4355, doi:10.1029/2002JD003190, 2003
- 12 Philip, S., Martin, R. V., van Donkelaar, A., J., Lo, Wai-Ho, J., Wang, Y., Chen, D.,
13 Zhang, L., Kasibhatla, P. S., Wang, S. W., Zhang, Q., Lu, Z., Streets, G. D.,
14 Bittman, S., and Macdonald, J. D.: Global Chemical Composition of Ambient
15 Fine Particulate Matter for Exposure Assessment, *Environ. Sci. Technol.*,
16 accepted, DOI: 10.1021/es502965b
- 17 Pungert, E. M. and West, J. J.: The effect of grid resolution on estimates of the burden
18 of ozone and fine particulate matter on premature mortality in the USA, *Air Qual.*
19 *Atmos. Health*, 6, 563–573, doi:10.1007/s11869-013-0197-8, 2013.
- 20 Qian, Y., Gustafson, W. I., Leung, L. R., and Ghan, S. J.: Effects of soot-induced snow
21 albedo change on snowpack and hydrological cycle in western United States
22 based on Weather Research and Forecasting chemistry and regional climate
23 simulations, *J. Geophys. Res.*, 114, D03108, doi:10.1029/2008JD011039, 2009
- 24 Ramanathan, V. and Carmichael, G.: Global and regional climate changes due to
25 black carbon, *Nature Geoscience*, 1, 221-227, 2008.
- 26 Randerson, J. T., Liu, H., Flanner, M. G., Chambers, S. D., Jin, Y., Hess, P. G., Pfister,
27 G., Mack, M. C., Treseder, K. K., Welp, L. R., Chapin, F. S., Harden, J. W.,
28 Goulden, M. L., Lyons, E., Neff, J. C., Schuur, E., Zender, C. S.: The impact of
29 boreal forest fire on climate warming, *Science*, 314, 1130-1132, 2006.
- 30 Ridley, D. A., Heald, L. C., and Ford, B.: North African dust export and deposition: A
31 satellite and model perspective, *J. Geophys. Res.*, 117, D02202,
32 doi:10.1029/2011JD016794, 2012.
- 33 Rodgers, C. D.: Inverse methods for atmospheric sounding, Series on Atmospheric,
34 Oceanic and Planetary Physics, vol. 2, World Scientific, Singapore, 2000.
- 35 Satheesh, S. K., Torres, O., Remer, L. A., Babu, S. S., Vinoj, V., Eck, T. F., Kleidman,
36 R. G., and Holben, B. N.: Improved assessment of aerosol absorption using
37 OMI-MODIS joint retrieval, *J. Geophys. Res.*, 114, D05209,
38 doi:10.1029/2008JD011024, 2009.
- 39 Satheesh, S. K., and Ramanathan, V.: Large differences in tropical aerosol forcing at
40 the top of the atmosphere and Earth's surface, *Nature*, 405, 60–63,
41 doi:10.1038/35011039, 2000
- 42 Schwartz, J., Coull, B., Laden, F., Ryan, L.: The effect of dose and timing of dose on
43 the association between airborne particles and survival. *Environ Health*
44 *Perspect* 116:64–69, 2008

- 1 Shen, Z., Liu, J., Horowitz, L. W., Henze, D. K., Fan, S., H., Levy II,
2 Mauzerall, D. L., Lin, J.-T., and Tao, S.: Analysis of transpacific transport of
3 black carbon during HIPPO-3: implications for black carbon aging, *Atmos.*
4 *Chem. Phys.*, 14, 6315-6327, doi:10.5194/acp-14-6315-2014, 2014.
- 5 Silva, A. R., West, J. J., Zhang, Y., Aneberg, C. S., Lamarque, J.-F., Shindell, T. D.,
6 Collins, J. W., Dalsoren, S., Faluvegl, G., Folbeth, G., Horowitz, W. L.,
7 Nagashima, T., Nalk, V., Rumbold, S., Skele, R., Sudo, K., Takemura, T.,
8 Bergmann, D., Camero-smith, P., Cionnl, I., Doherty, M. R., Eyring, V., Josse,
9 B., MacKenzie, I. A., Plummer, D., Righl, M., Stevenson, S. D., Strode, S.,
10 Szopa, S., Zeng, G.: Global premature mortality due to anthropogenic outdoor
11 air pollution and the contribution of past climate change. *Environ. Res. Lett.* 8,
12 034005 doi:10.1088/1748-9326/8/3/034005, 2013.
- 13 Sinyuk, A, Dubovik, O., Holben, B., Eck, T. F., Breon, F. M., Martonchik, J., Kahn,
14 R., Diner, D. J., Vermote, E. F., Roger, J. C., Lapyonok, T., Slutsker, I.:
15 Simultaneous retrieval of aerosol and surface properties from a combination of
16 AERONET and satellite data. *Remote Sens. Environ.*, 107(2-Jan), 90-108, 2007.
- 17 Stier, P., Seinfeld J. H., Kinne, S., Feichter, J., and Boucher, O.: Impact of
18 nonabsorbing anthropogenic aerosols on clear-sky atmospheric absorption, *J.*
19 *Geophys. Res.*, 111, D18201, doi:10.1029/2006JD007147, 2006.
- 20 Textor, C., Schulz, M., Guibert, S., Kinne, S., Balkanski, Y., Bauer, S., Berntsen, T.,
21 Berglen, T., Boucher, O., Chin, M., Dentener, F., Diehl, T., Feichter, J.,
22 Fillmore, D., Ginoux, P., Gong, S., Grini, A., Hendricks, J., Horowitz, L.,
23 Huang, P., Isaksen, I. S. A., Iversen, T., Kloster, S., Koch, D., Kirkevåg, A.,
24 Kristjansson, J. E., Krol, M., Lauer, A., Lamarque, J. F., Liu, X., Montanaro, V.,
25 Myhre, G., Penner, J. E., Pitari, G., Reddy, M. S., Seland, Ø., Stier, P.,
26 Takemura, T., and Tie, X.: The effect of harmonized emissions on aerosol
27 properties in global models – an AeroCom experiment, *Atmos. Chem. Phys.*, 7,
28 4489-4501, doi:10.5194/acp-7-4489-2007, 2007.
- 29 Torres, O., Ahn, C., and Chen, Z.: Improvements to the OMI near-UV aerosol
30 algorithm using A-train CALIOP and AIRS observations, *Atmos. Meas. Tech.*,
31 6, 3257-3270, doi:10.5194/amt-6-3257-2013, 2013.
- 32 Torres, O., Bhartia, P. K., Herman, J. R., and Ahmad, Z.: Derivation of aerosol
33 properties from satellite measurements of backscattered ultraviolet radiation.
34 Theoretical Basis, *J. Geophys. Res.*, 103(D14), 17,099– 17,110,
35 doi:10.1029/98JD00900, 1998.
- 36 Torres, O., Bhartia, P. K., Sinyuk, A., Welton, E. J., and Holben, B.: Total Ozone
37 Mapping Spectrometer measurements of aerosol absorption from space:
38 Comparison to SAFARI 2000 ground-based observations, *J. Geophys. Res.*,
39 110, D10S18, doi:10.1029/2004JD004611, 2005.
- 40 Torres, O., Tanskanen, A., Veihelmann, B., Ahn, C., Braak, R., Bhartia, P. K.,
41 Veefkind, P., and Levelt P.: Aerosols and surface UV products from Ozone
42 Monitoring Instrument observations: An overview, *J. Geophys. Res.*, 112,
43 D24S47, doi:10.1029/2007JD008809, 2007.
- 44 United Nations Environment Program and World Meteorological Organization,

- 1 “Integrated Assessment of Black Carbon and Tropospheric Ozone” (Nairobi,
2 2011).
- 3 van der Werf, G. R., Randerson, J. T., Giglio, L., Collatz, G. J., Kasibhatla, P. S., and
4 Arellano Jr., A. F.: Interannual variability in global biomass burning emissions
5 from 1997 to 2004, *Atmos. Chem. Phys.*, 6, 3423-3441, doi:10.5194/acp-6-
6 3423-2006, 2006.
- 7 van der Werf, G. R., Randerson, J. T., Giglio, L., Collatz, G. J., Mu, M., Kasibhatla, P.
8 S., Morton, D. C., DeFries, R. S., Jin, Y., and van Leeuwen, T. T.: Global fire
9 emissions and the contribution of deforestation, savanna, forest, agricultural,
10 and peat fires (1997–2009), *Atmos. Chem. Phys.*, 10, 11707–11735, doi:
11 10.5194/acp-10-11707-2010, 2010.
- 12 van Donkelaar, A., Martin, R. V., Spurr, R. J. D., Drury, E., Remer, L. A., Levy, R.
13 C., and Wang, J., Optimal estimation for global ground-level fine particulate
14 matter concentrations, *J. Geophys. Res. Atmos.*, 118, 5621–5636,
15 doi:10.1002/jgrd.50479,2013
- 16 Wang, J., Xu, X., Henze, K. D., Zeng, J., Ji, Q., Tsay, S.-C., and Huang, J.: Top-down
17 estimate of dust emissions through integration of MODIS and MISR aerosol
18 retrievals with the GEOS-Chem adjoint model, *Geophys. Res. Lett.*, 39,
19 L08802, doi:10.1029/2012GL051136, 2012.
- 20 Wang, Q., Jacob, D. J., Fisher, J. A., Mao, J., Leibensperger, E. M., Carouge, C. C.,
21 Le Sager, P., Kondo, Y., Jimenez, J. L., Cubison, M. J., and Doherty, S. J.:
22 Sources of carbonaceous aerosols and deposited black carbon in the Arctic in
23 winter-spring: implications for radiative forcing, *Atmos. Chem. Phys.*, 11,
24 12453-12473, doi:10.5194/acp-11-12453-2011, 2011.
- 25 Wang, X., Wang, Y., Hao, J., Kondo, Y., Irwin, M., Munger, J. W., and Zhao, Y.: Top-
26 down estimate of China’s black carbon emissions using surface observations:
27 Sensitivity to observation representativeness and transport model error, *J.*
28 *Geophys. Res. Atmos.*, 118, 5781–5795, doi:10.1002/jgrd.50397, 2013.
- 29 Wang, Y. X., McElroy, B. M., Jacob, J. D., and Yantosca, R. M.: A nested grid
30 formulation for chemical transport over Asia: Applications to CO, *J. Geophys.*
31 *Res.*, 109, D22307, doi:10.1029/2004JD005237, 2004.
- 32 Wang, Y., Jacob, J. D., and Logan, A. J.: Global simulation of tropospheric O₃-NO_x-
33 hydrocarbon chemistry, 1. Model formulation, *J. Geophys. Res.*, 103/D9,
34 10,713-10,726, 1998.
- 35 Wecht, K. J., J. D., Jacob, Wofsy, C. S., Kort, A. E., Worden, R. J., Kulawik, S. S.,
36 Henze, K. D., Kopacz, M., and Payne, H. V.: Validation of TES methane with
37 HIPPO aircraft observations: implications for inverse modeling of methane
38 sources, *Atmos. Chem. Phys.*, 12, 1823-1832, 2012.
- 39 Wecht, K. J., Jacob, J. D., Frankenberg, C., Jiang, Z., and Blake, D. R.: Mapping of
40 North American methane emissions with high spatial resolution by inversion of
41 SCIAMACHY satellite data, *J. Geophys. Res. Atmos.*, 119, 7741–7756
42 doi:10.1002/2014JD021551, 2014
- 43 Wesely, M. L.: Parameterization of surface resistance to gaseous dry deposition in
44 regional-scale numerical models, *Atmos. Environ.*, 23, 1293-1304, 1989.

1 Worden, H. M., Logan, J. A., Worden, J. R., Beer, R., Bowman, K., Clough, S. A.,
2 Eldering, A., Fisher, B. M., Gunson, M. R., Herman, R. L., Kulawik, S. S.,
3 Lampel, M. C., Luo, M., Meqretskaiia, I. A., Osterman, G. B., Shephard, M. W.:
4 Comparisons of Tropospheric Emission Spectrometer (TES) ozone profiles to
5 ozonesondes: Methods and initial results, *J. Geophys. Res.*, 112, D03309,
6 doi:10.1029/2006JD007258, 2007.

7 Xu, X., Wang, J., Henze, K. D., Qu, W., Kopacz, M.: Constraints on Aerosol Sources
8 Using GEOS-Chem Adjoint and MODIS Radiances, and Evaluation with Multi-
9 sensor (OMI, MISR) data, *J. Geophys. Res.*, 118, 6396–6413
10 doi:10.1002/jgrd.50515, 2013

11 Zhang L., Liao, H., Li, J.: Impacts of Asian Summer Monsoon on Seasonal and
12 Interannual Variations of Aerosols over Eastern China. *J. Geophys. Res.*, 115,
13 D00K05, doi:10.1029/2009JD012299, 2010.

14 Zhang, L., Jacob, J. D., Kopacz, M. Henze, K. D., Singh, K., and Jaffe, D. A.:
15 Intercontinental source attribution of ozone pollution at western U.S. sites using
16 an adjoint method, *Geophys. Res. Lett.*, 36, L11810,
17 doi:10.1029/2009GL037950, 2009.

18 Zhang, L., Kok, J., Henze, K. D., Li, Q. B., and Zhao, C.: Improving simulations of
19 fine dust surface concentrations over the Western United States by optimizing
20 the particle size distribution, *Geophys. Res. Lett.*, 40, 3270–3275, doi:
21 10.1002/grl.50591, 2013.

22 Zhang, Q., Streets, D. G., Carmichael, G. R., He, K. B., Huo, H., Kannari, A.,
23 Klimont, Z., Park, I. S., Reddy, S., Fu, J. S., Chen, D., Duan, L., Lei, Y., Wang,
24 L. T., and Yao, Z. L.: Asian emissions in 2006 for the NASA INTEX-B mission,
25 *Atmos. Chem. Phys.*, 9, 5131-5153, 2009.

26 Zhang, X. Y., Wang, Y. Q., Zhang, X. C., Guo, W., Gong, S. L., Zhao, P., and Jin, J.
27 L.: Carbonaceous aerosol composition over various regions of China during
28 2006, *J. Geophys. Res.*, 113, D14111, doi:10.1029/2007JD009525, 2008

29 Zhao, C., Liu, X., Leung, L. R., Johnson, B., McFarlane, S. A., Gustafson Jr., W. I.,
30 Fast, J. D., and Easter, R.: The spatial distribution of mineral dust and its
31 shortwave radiative forcing over North Africa: modeling sensitivities to dust
32 emissions and aerosol size treatments, *Atmos. Chem. Phys.*, 10, 8821-8838,
33 doi:10.5194/acp-10-8821-2010, 2010.

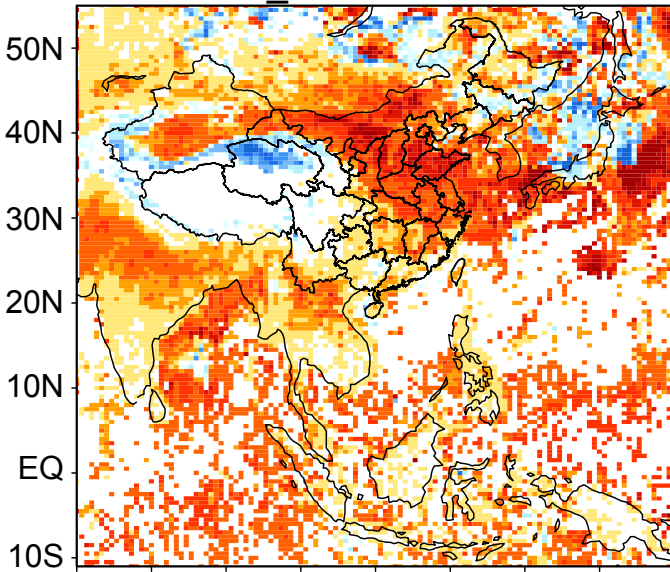
34 Zhu, C., Byrd, R. H., Lu, P., and Nocedal, J.: L-BFGS-B: A limited memory
35 FORTRAN code for solving bound constrained optimization problems, *Tech.*
36 *Rep.*, Northwestern University, 1994

37 Zhu, L., Henze, K. D., Cady-Pereira, K. E., Shephard, M. W., Luo, M., Pinder, R. W.,
38 Bash, J. O., Jeong, G.: Constraining U.S. ammonia emissions using TES remote
39 sensing observations and the GEOS-Chem adjoint model, *J. Geophys. Res.*, 118,
40 3355–3368, doi:10.1002/jgrd.50166, 2013.

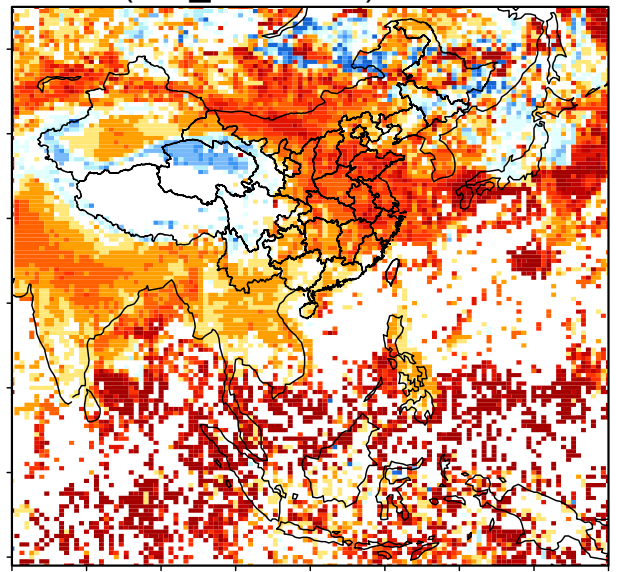
41

April

GC_OMI minus OMI



(GC_OMI-OMI)/OMI %



October

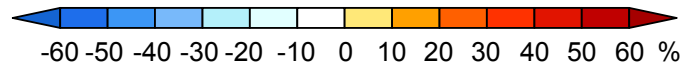
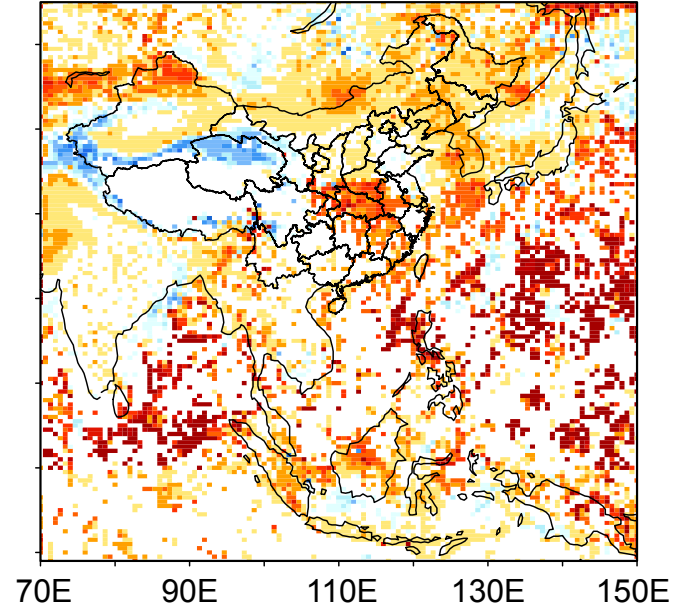
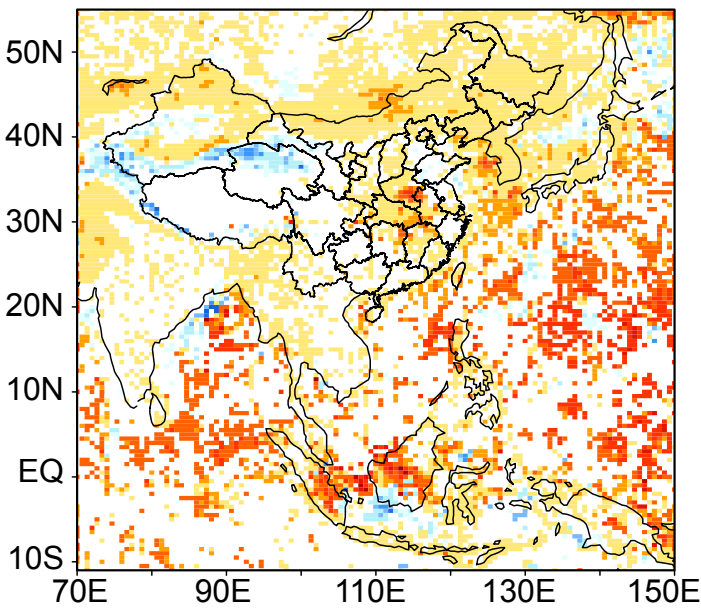


Fig. 1

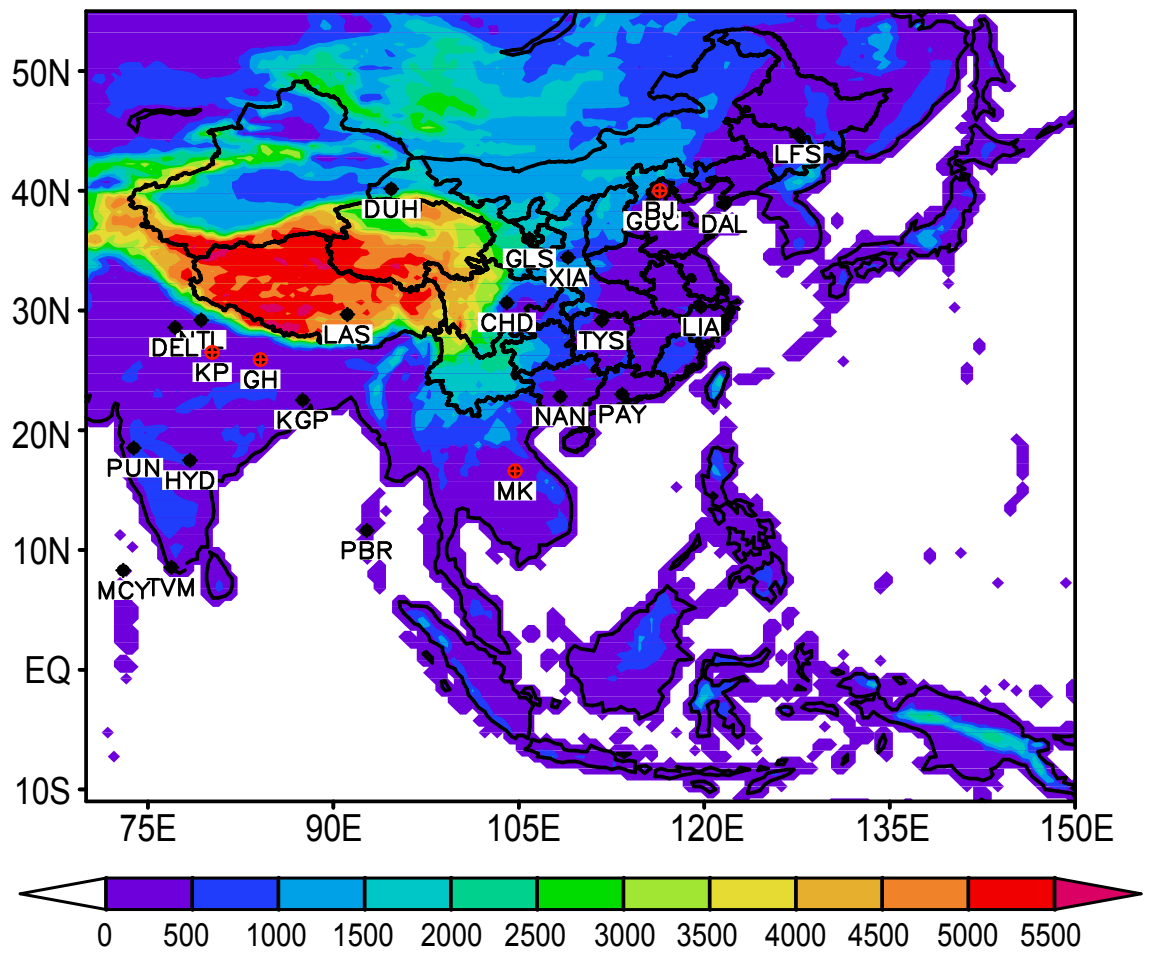


Fig. 2

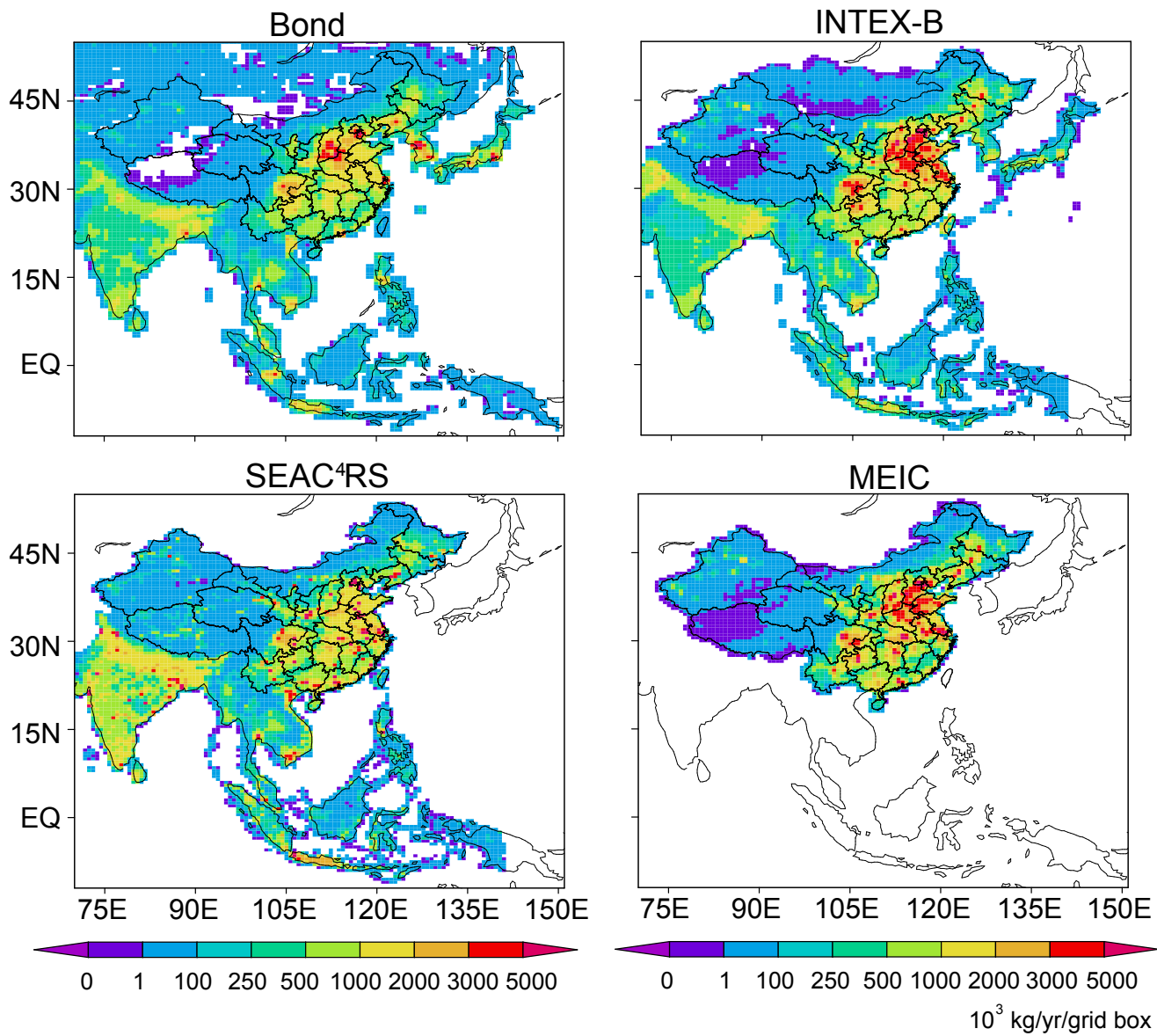


Fig. 3

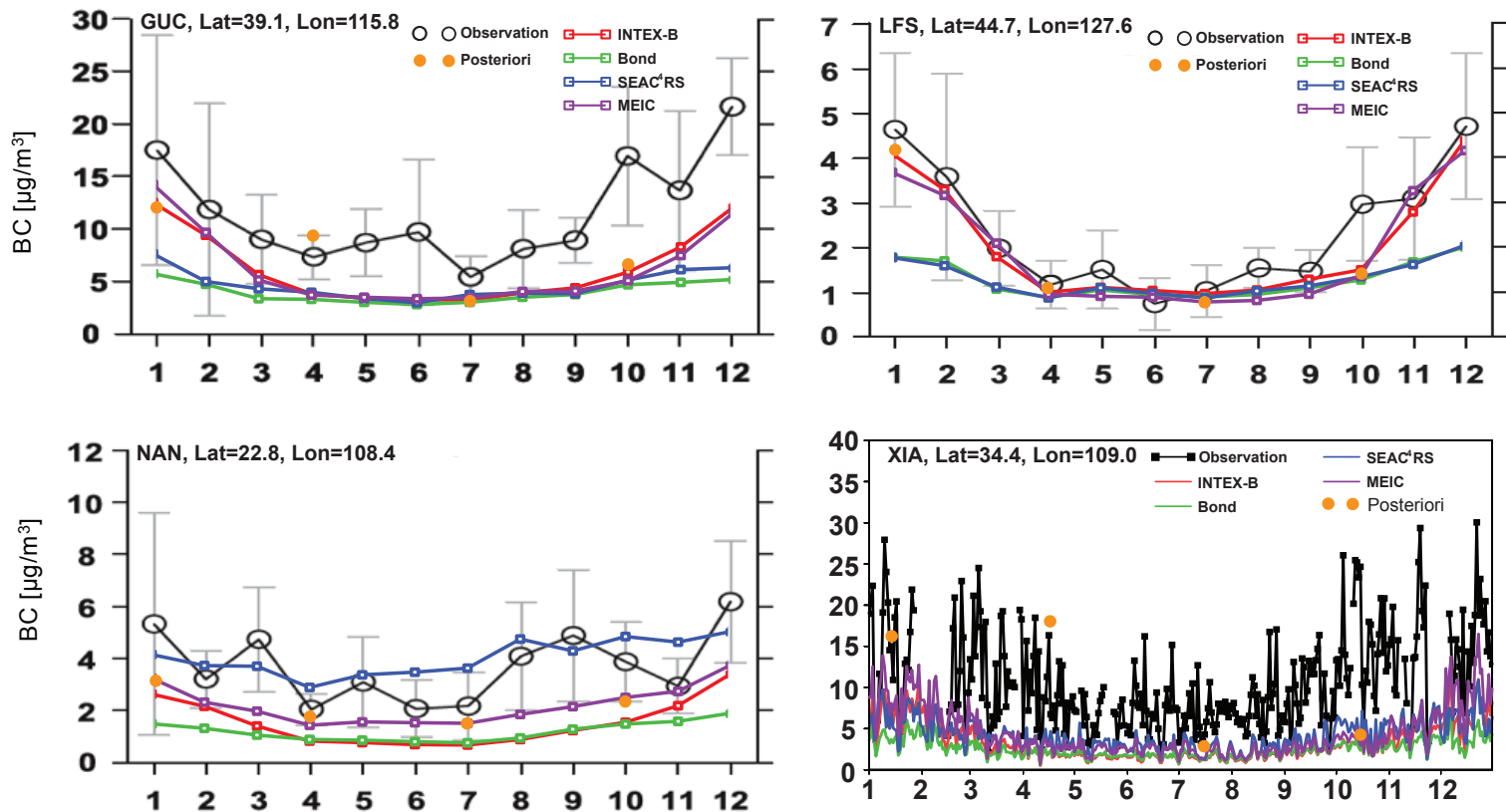
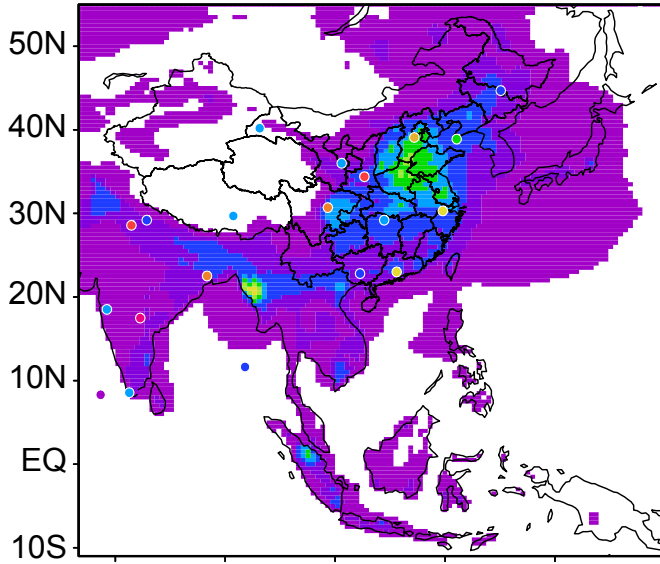


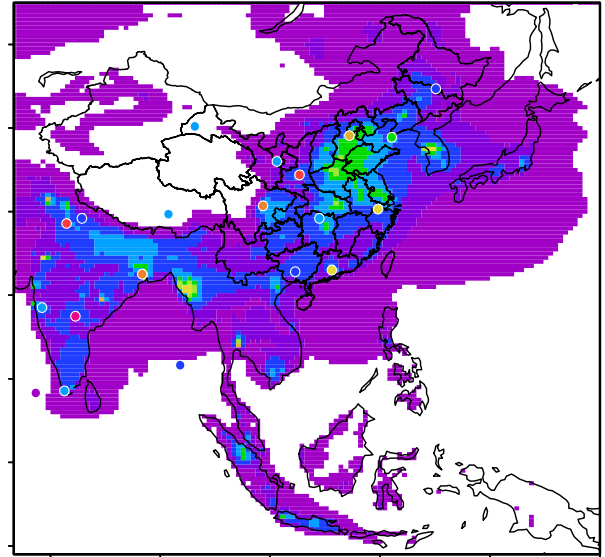
Fig. 4

April

INTEX-B



MEIC_SEAC⁴RS



October

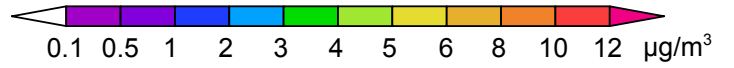
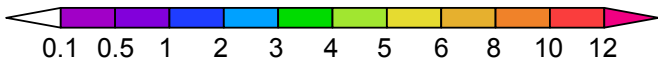
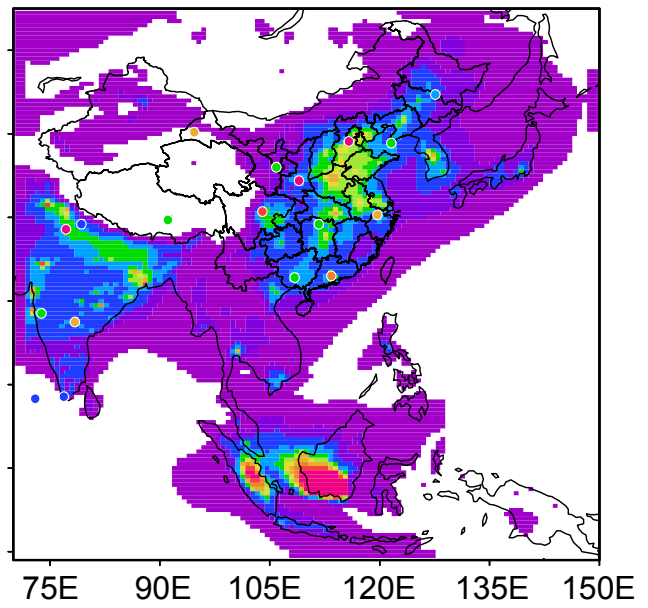
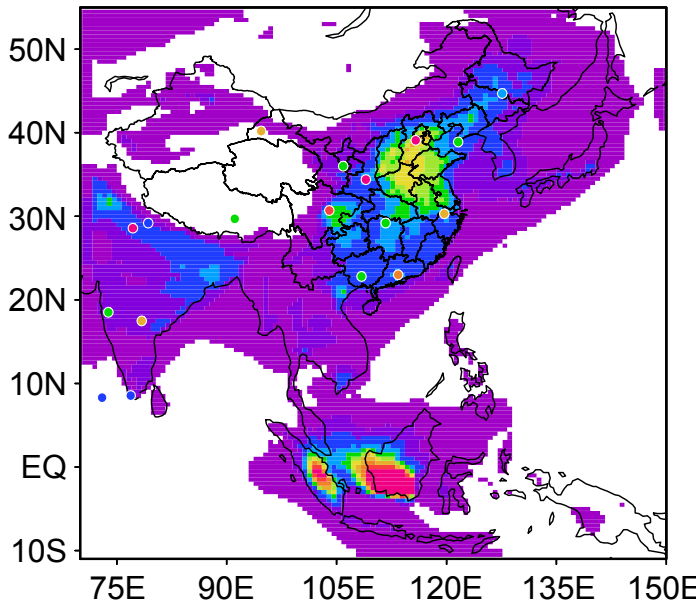
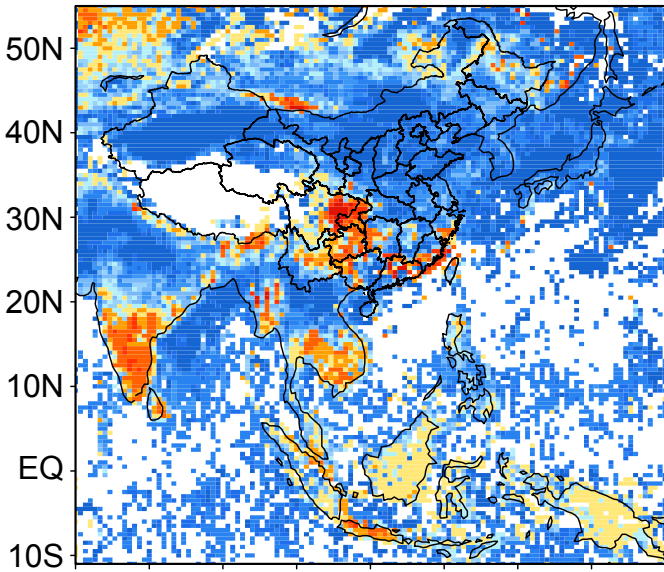
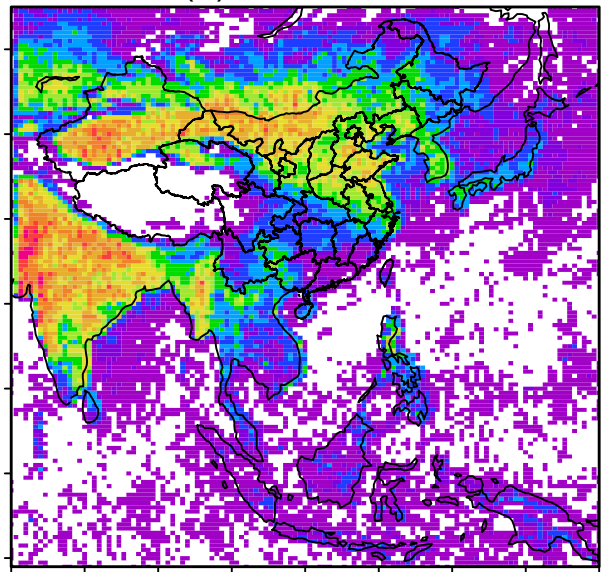


Fig. 5

April (a) GEOS-Chem minus OMI



(b) Data counts



October

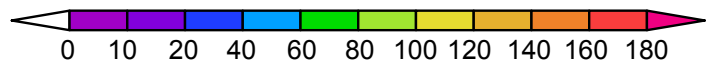
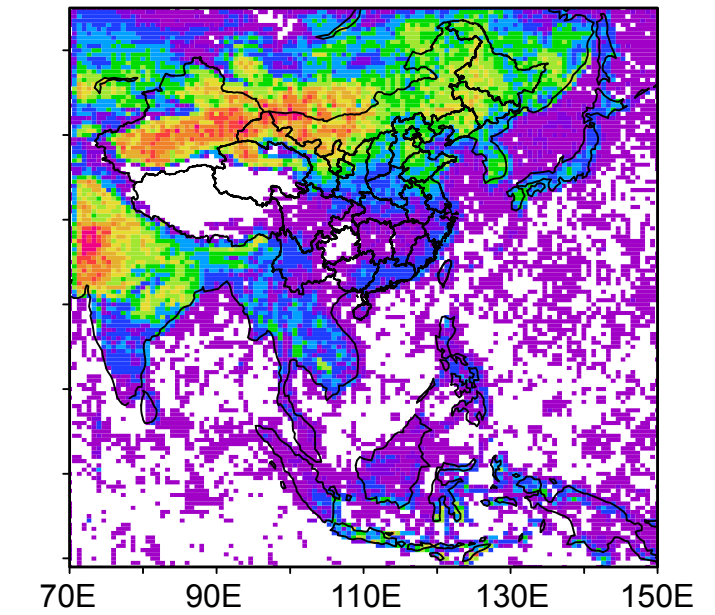
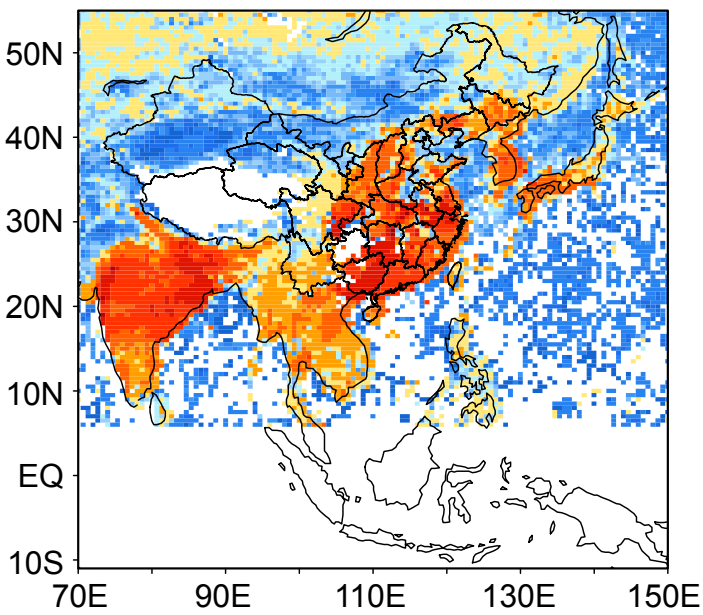


Fig. 6

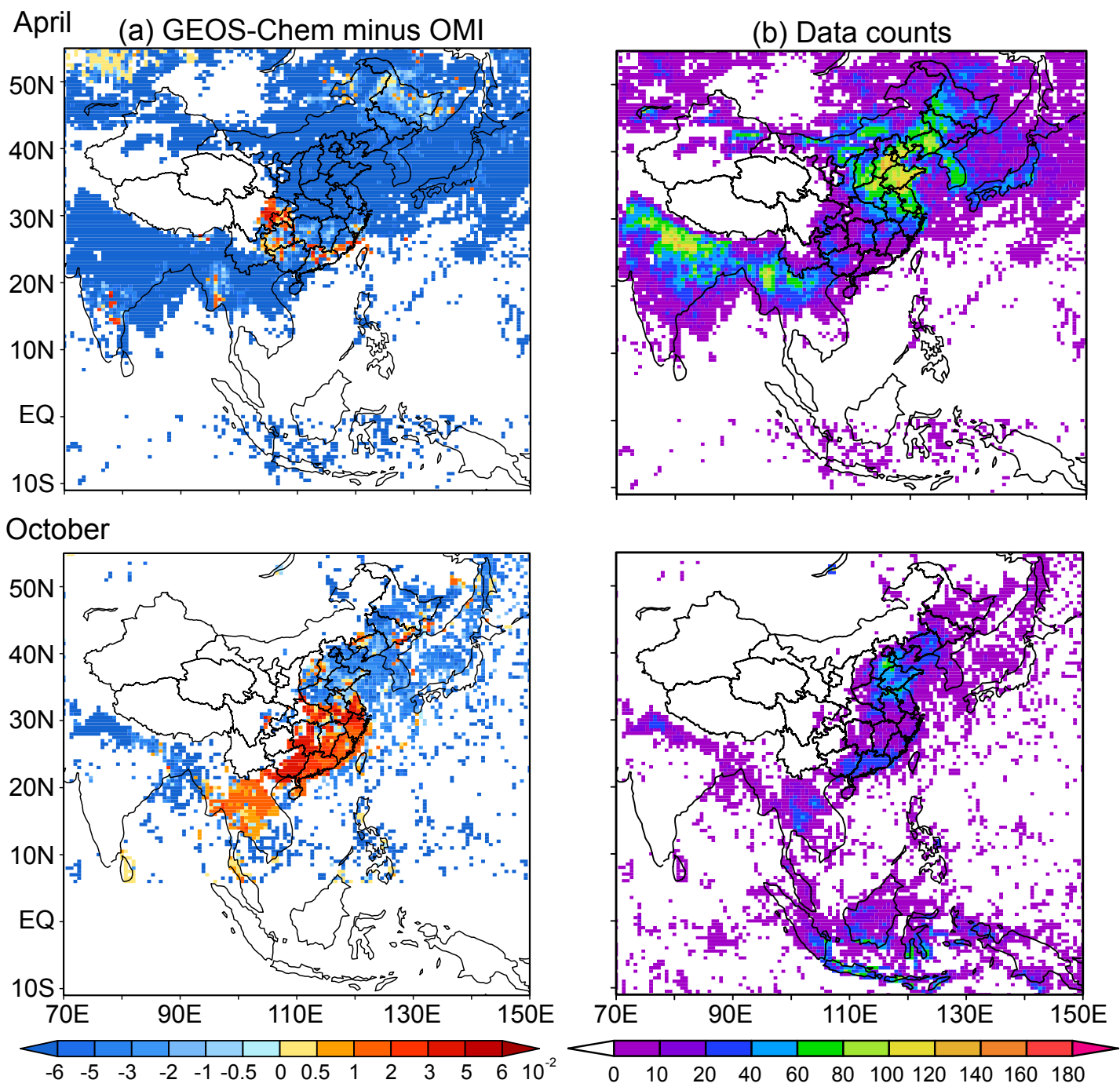


Fig. 7

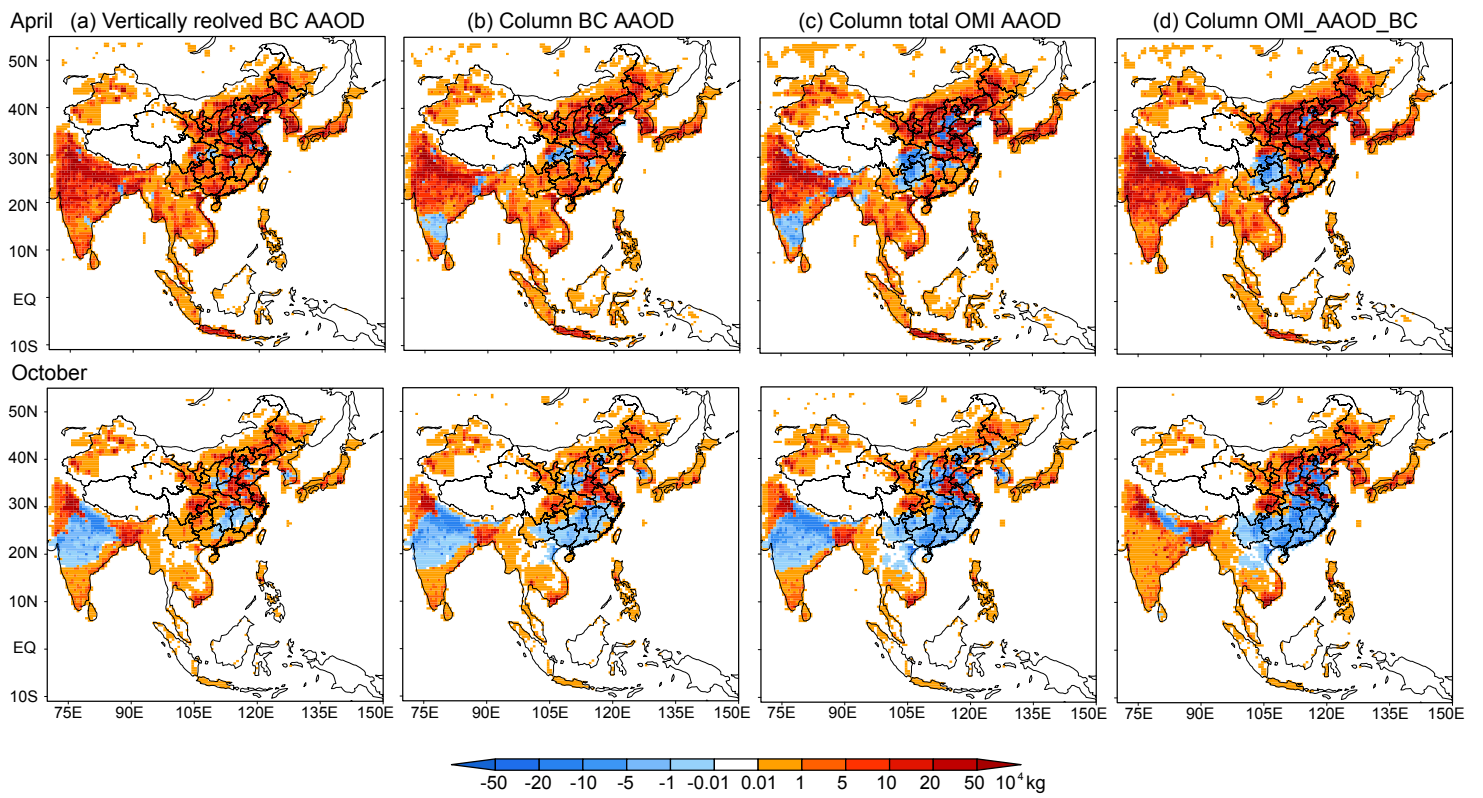


Fig. 8

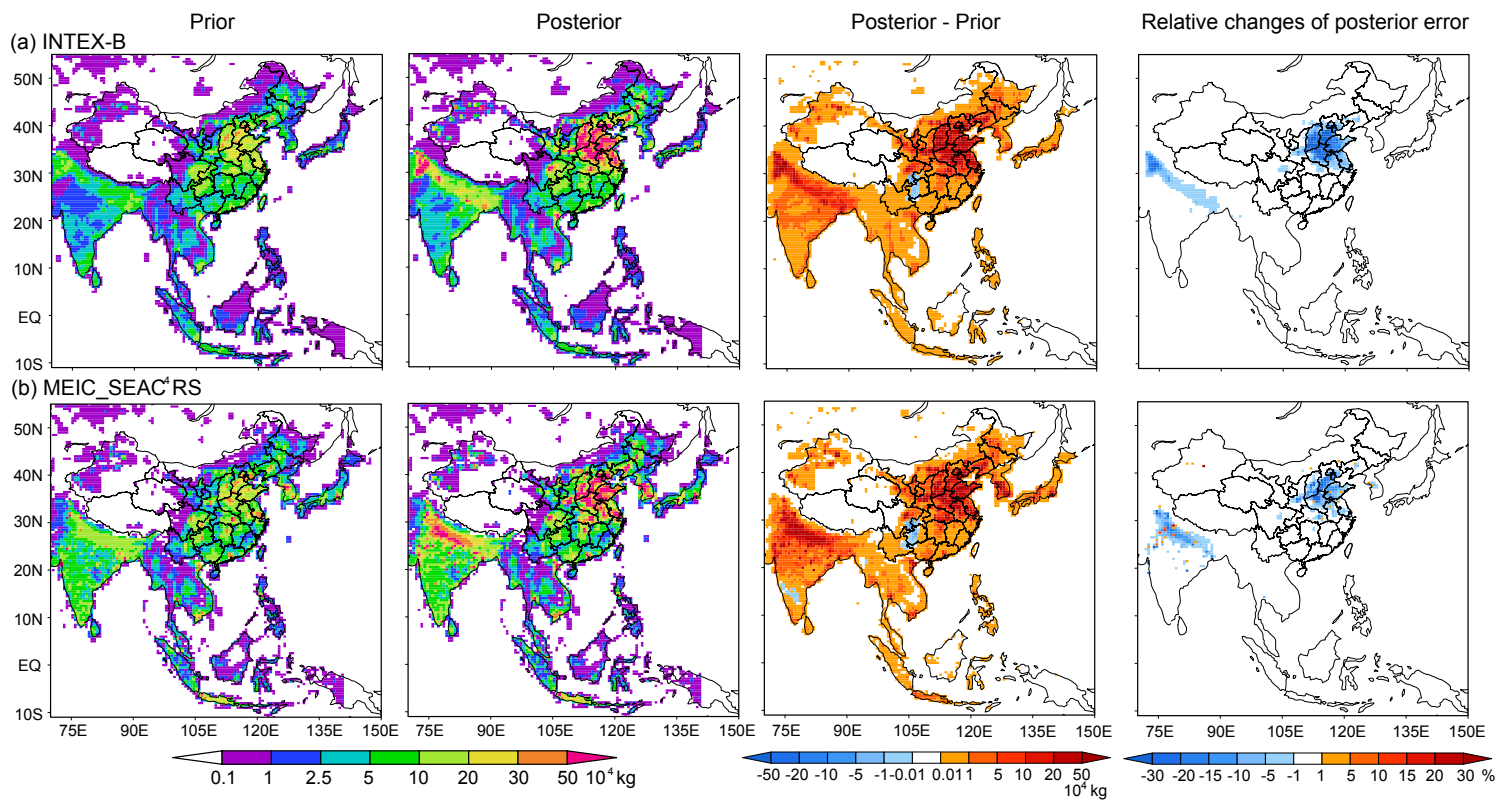


Fig. 9

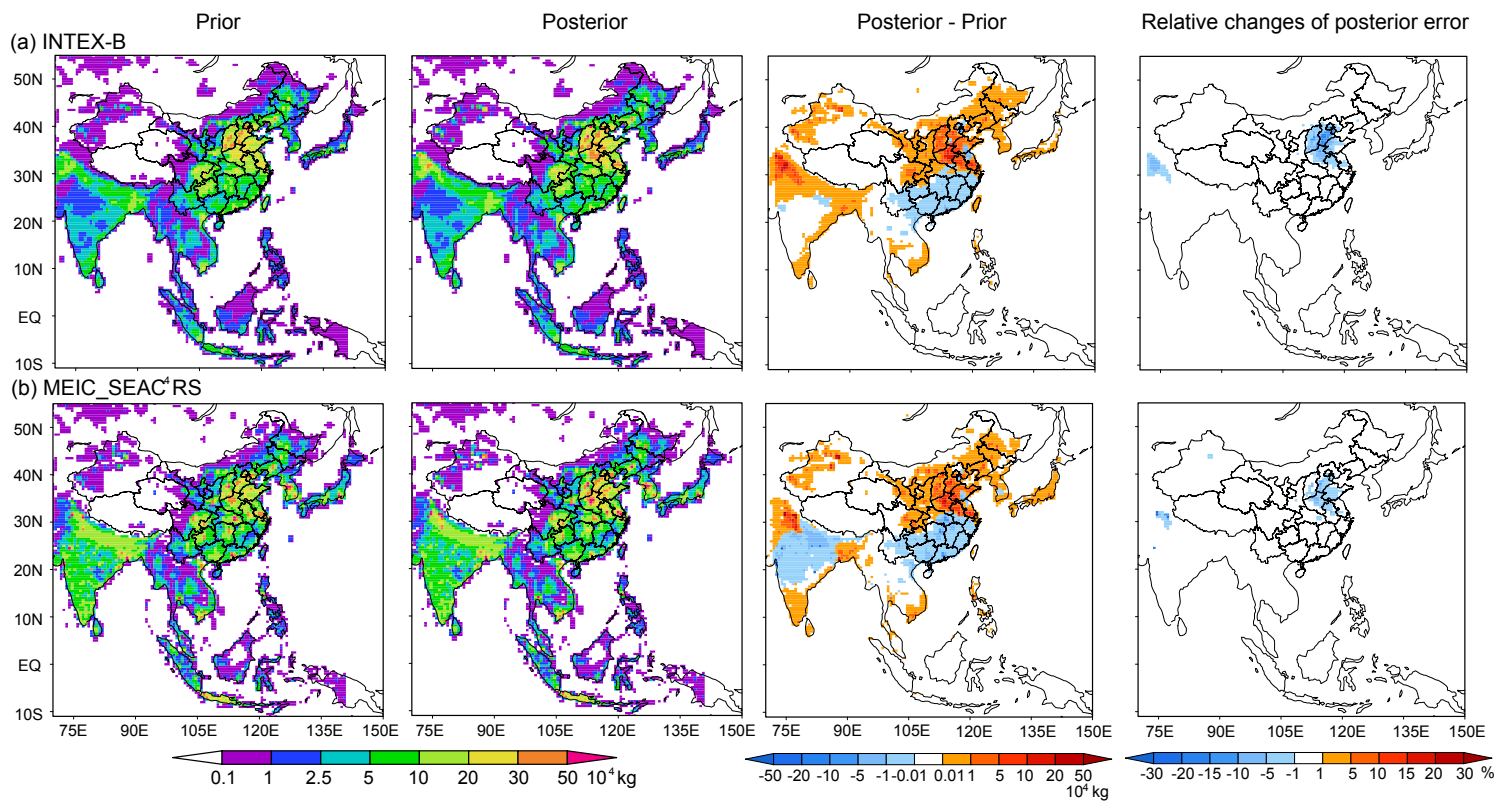


Fig. 10

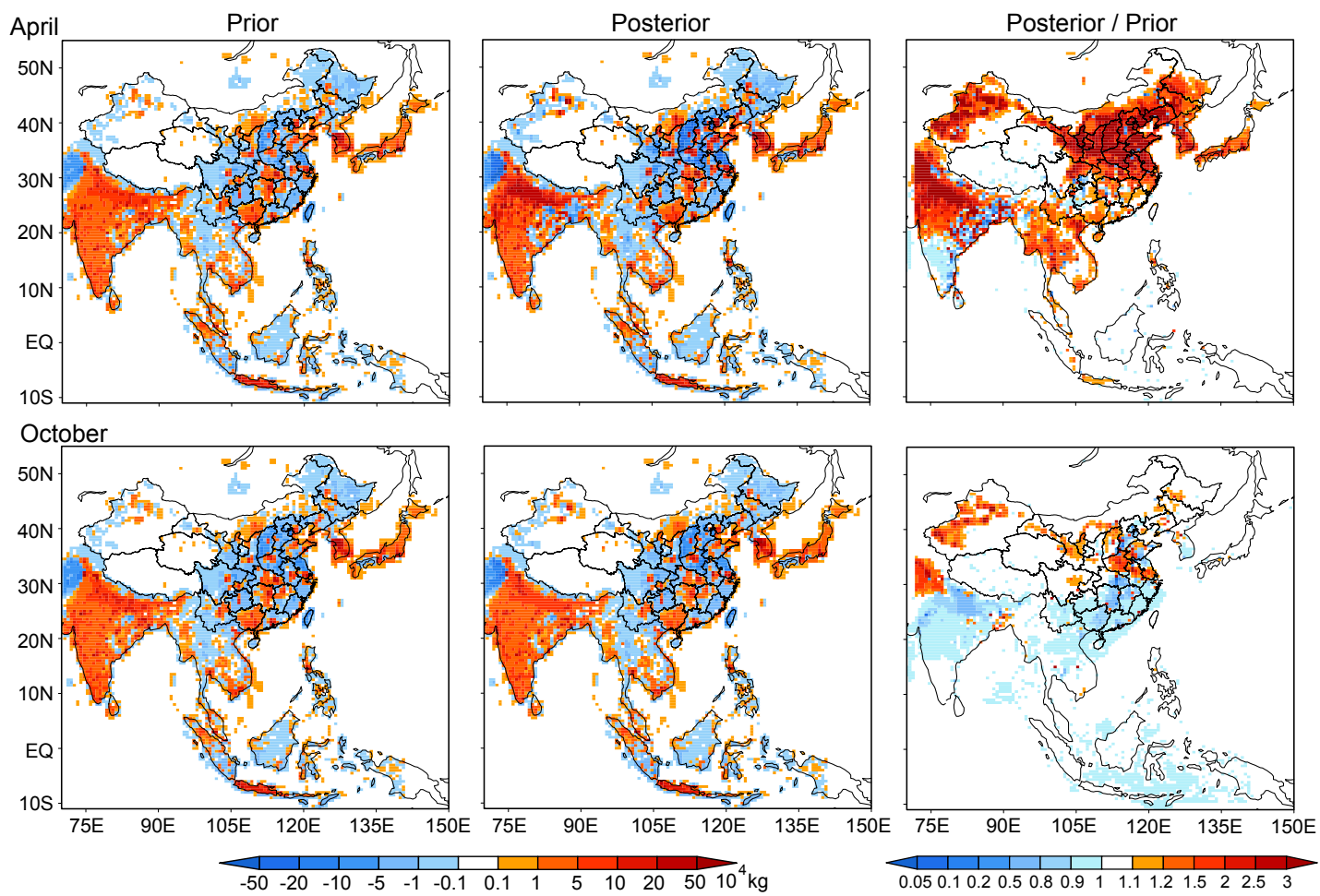


Fig. 11

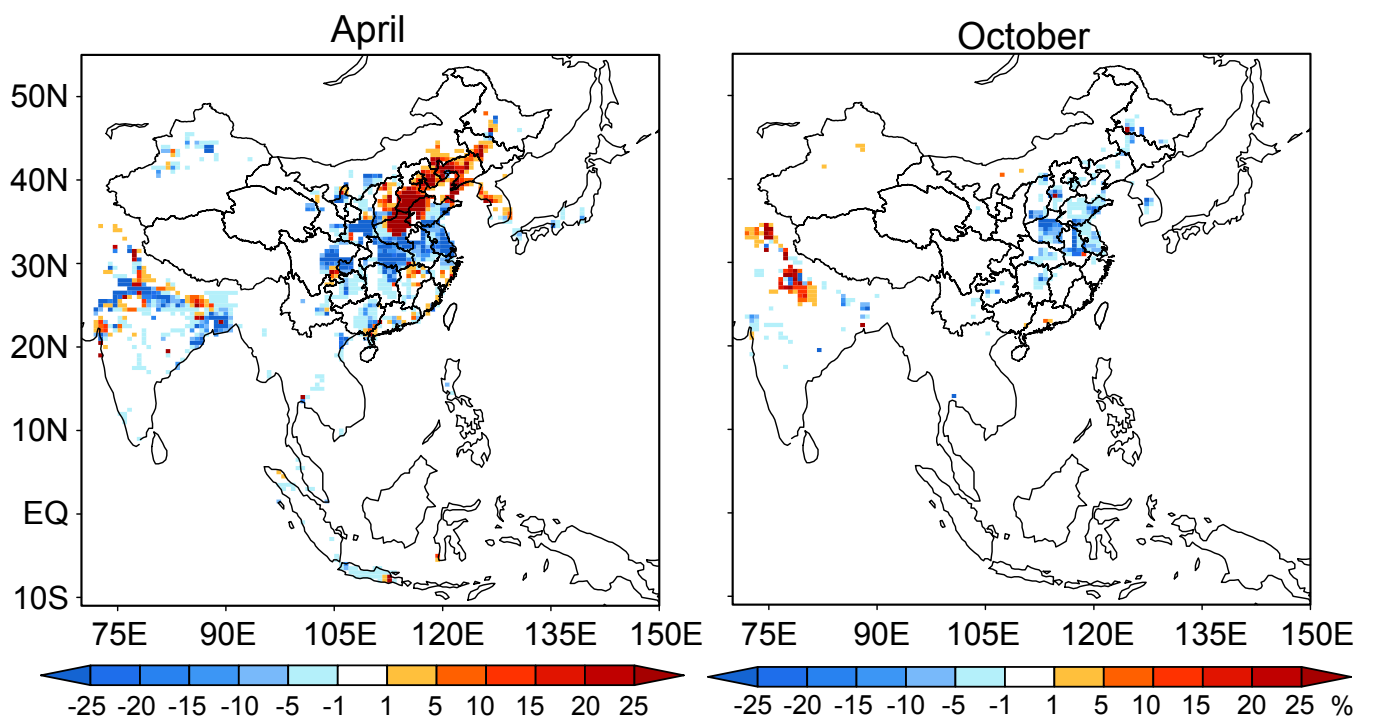
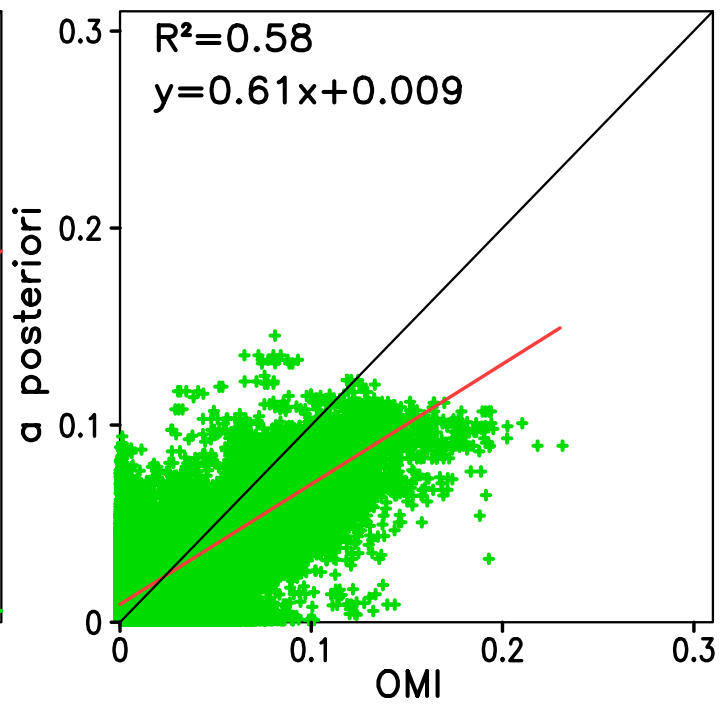
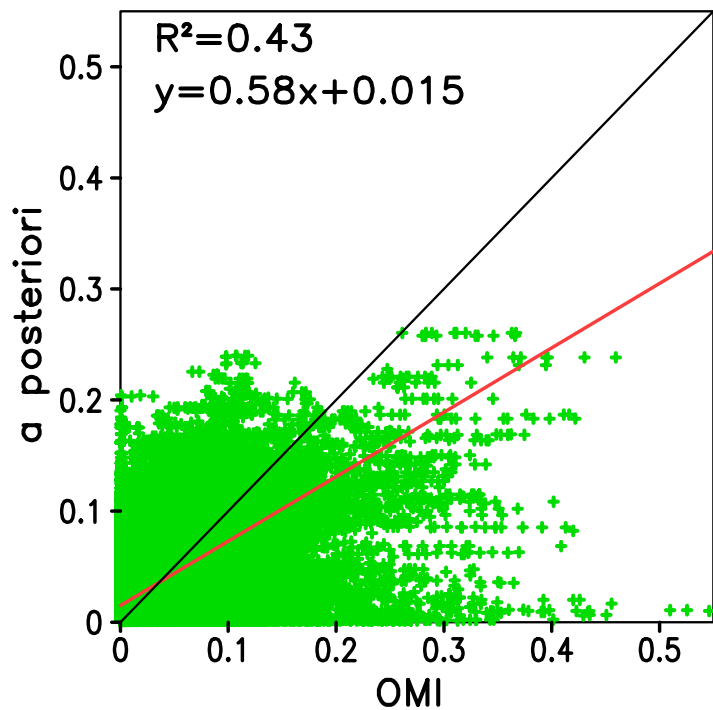
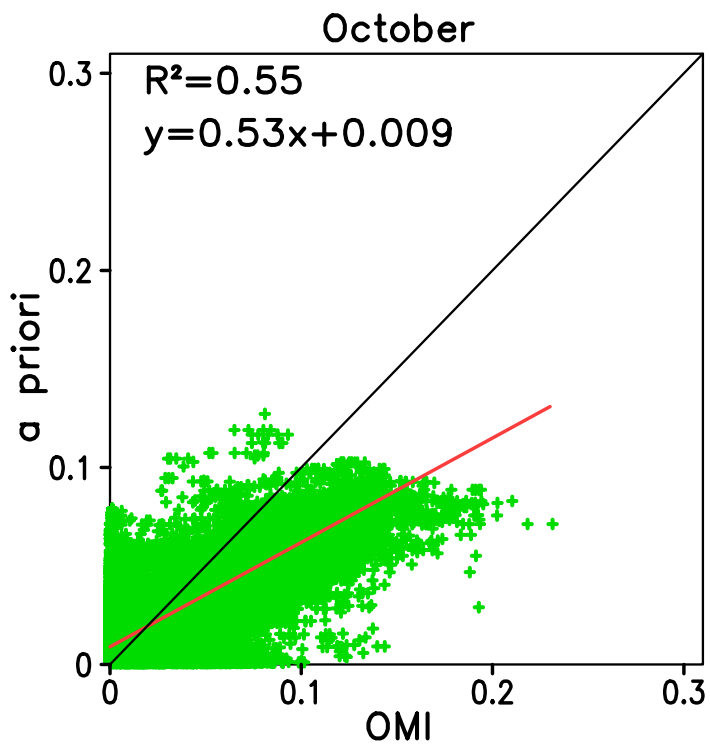
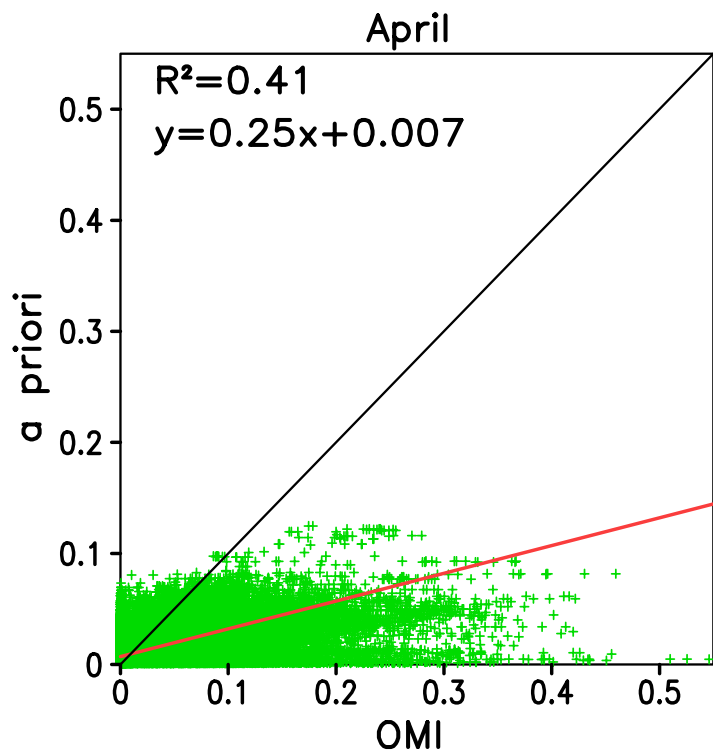
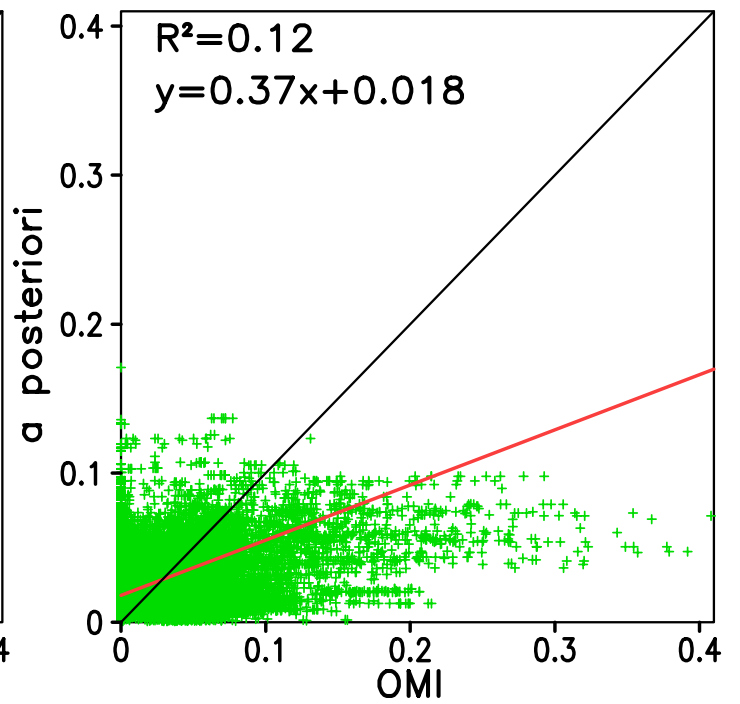
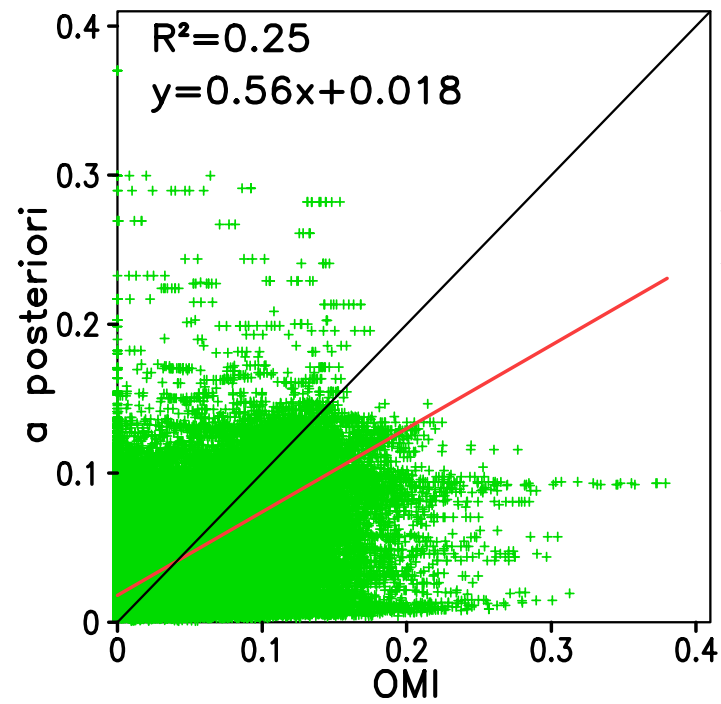
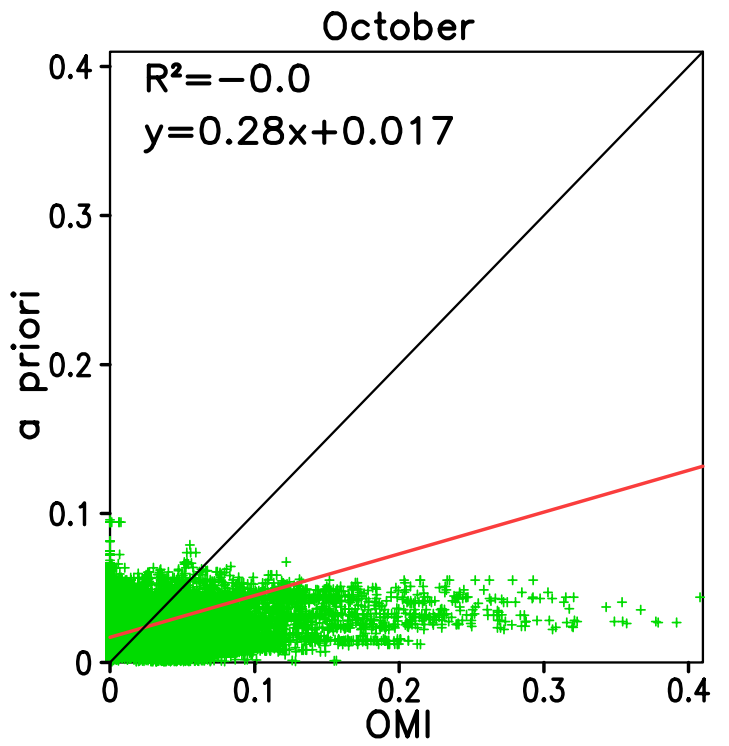
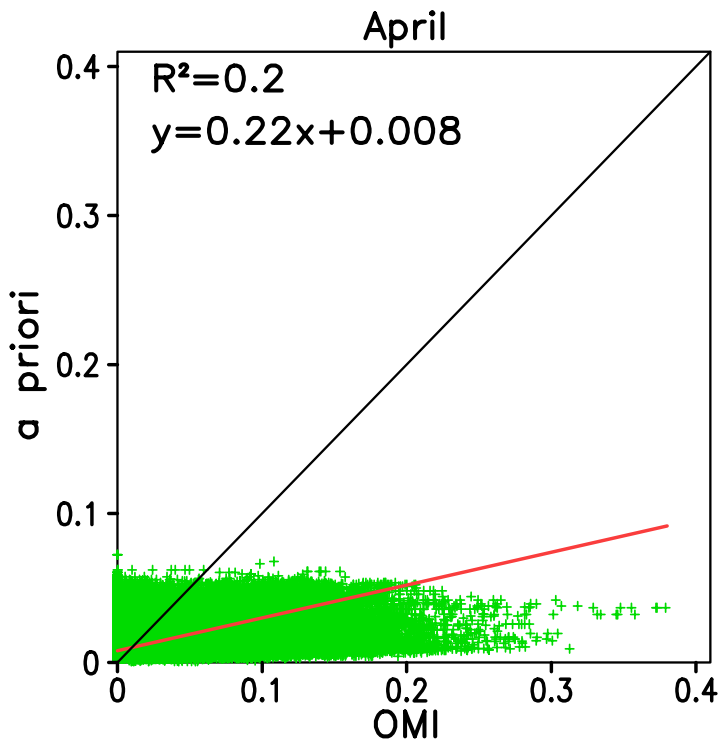


Fig. 12





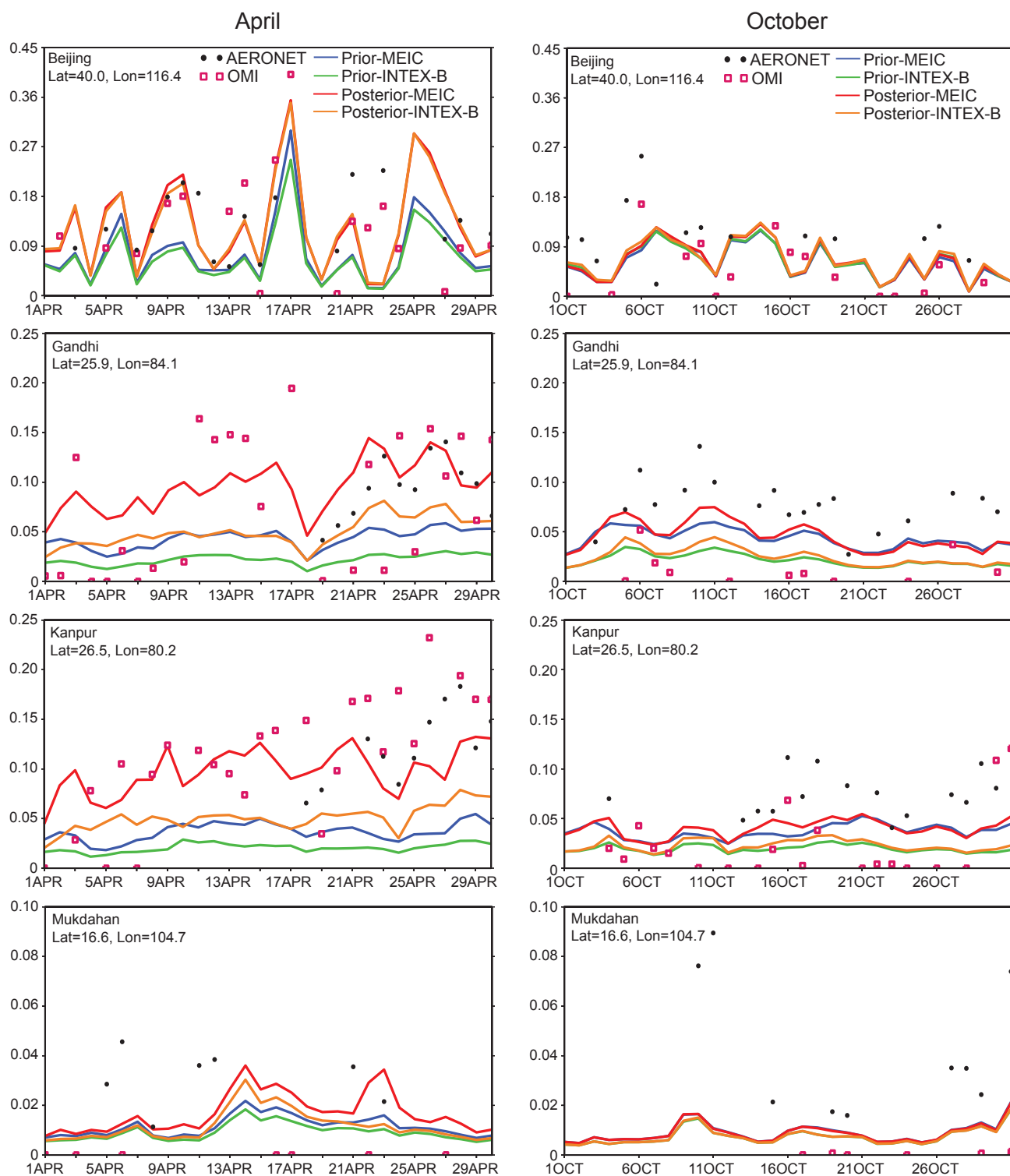
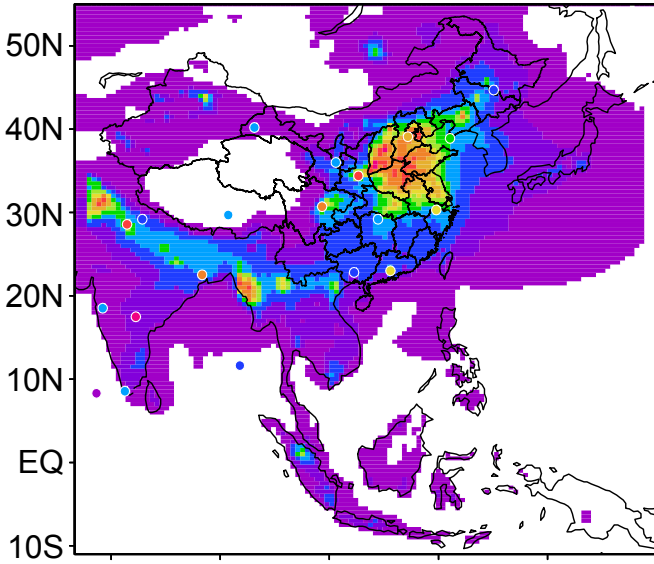


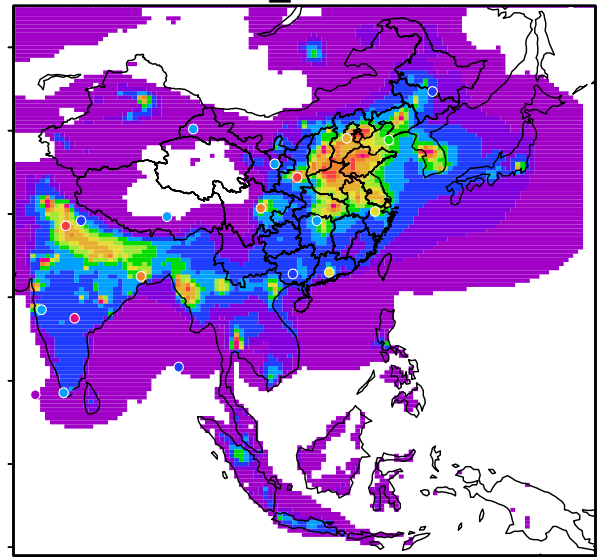
Fig. 15

April

INTEX-B



MEIC_SEAC⁴RS



October

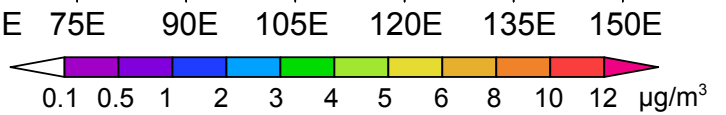
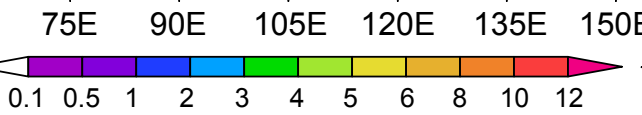
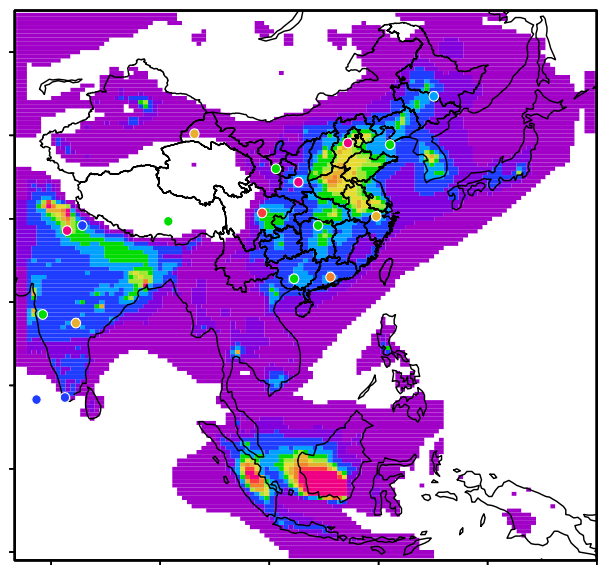
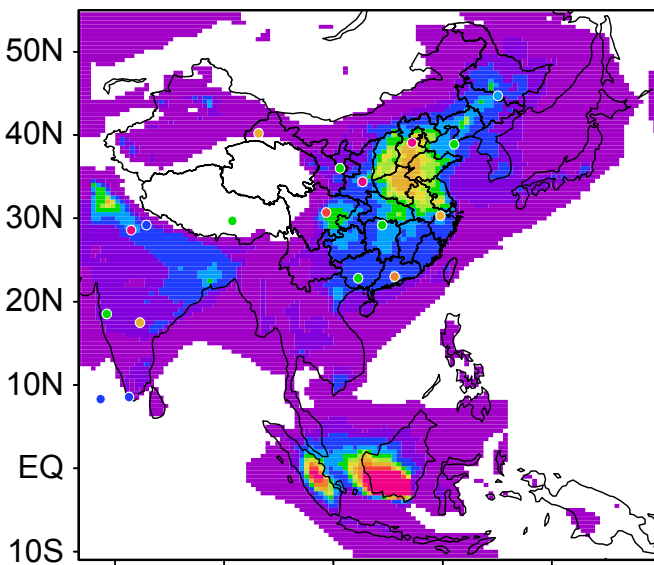


Fig. 16

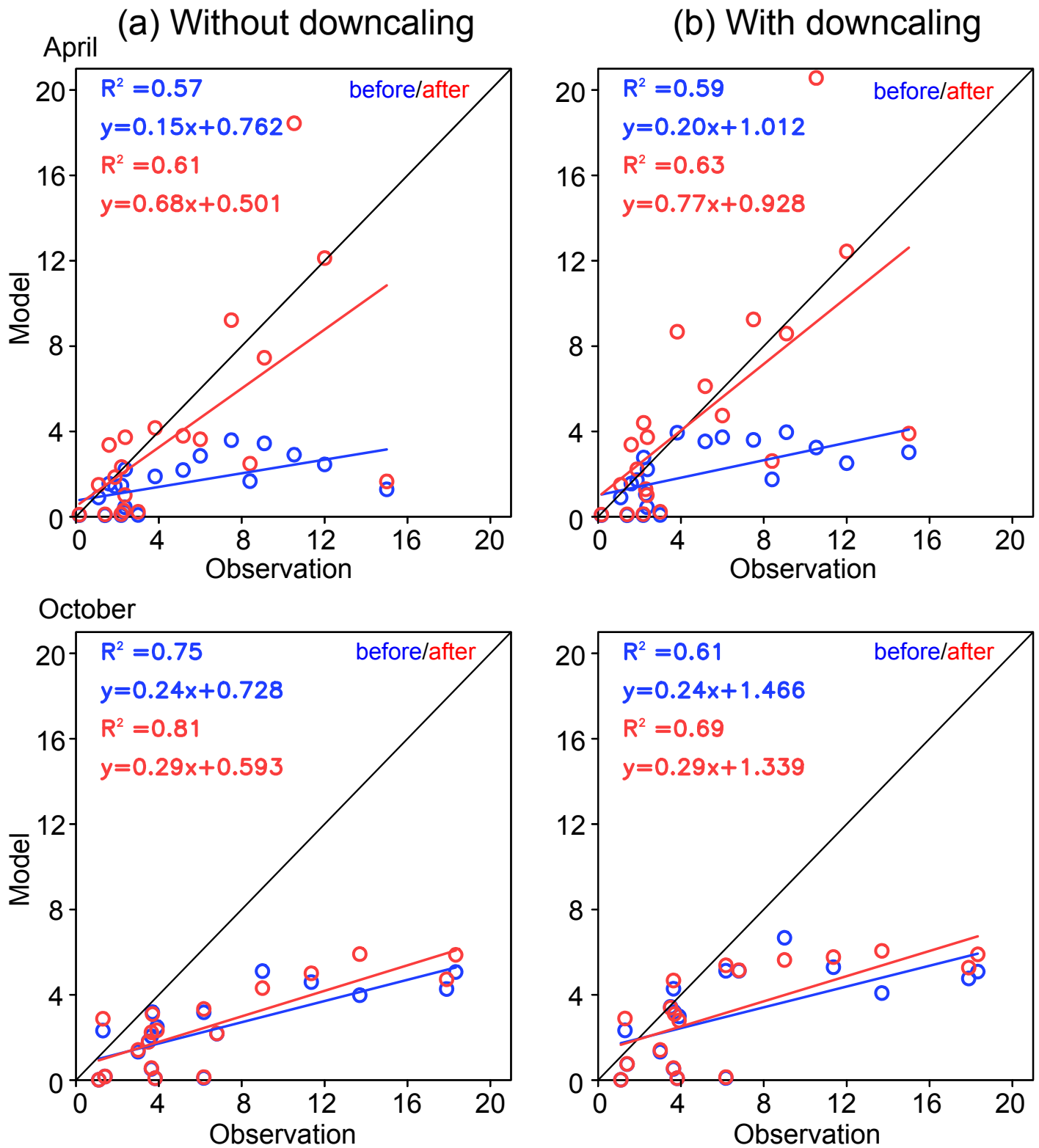


Fig. 17

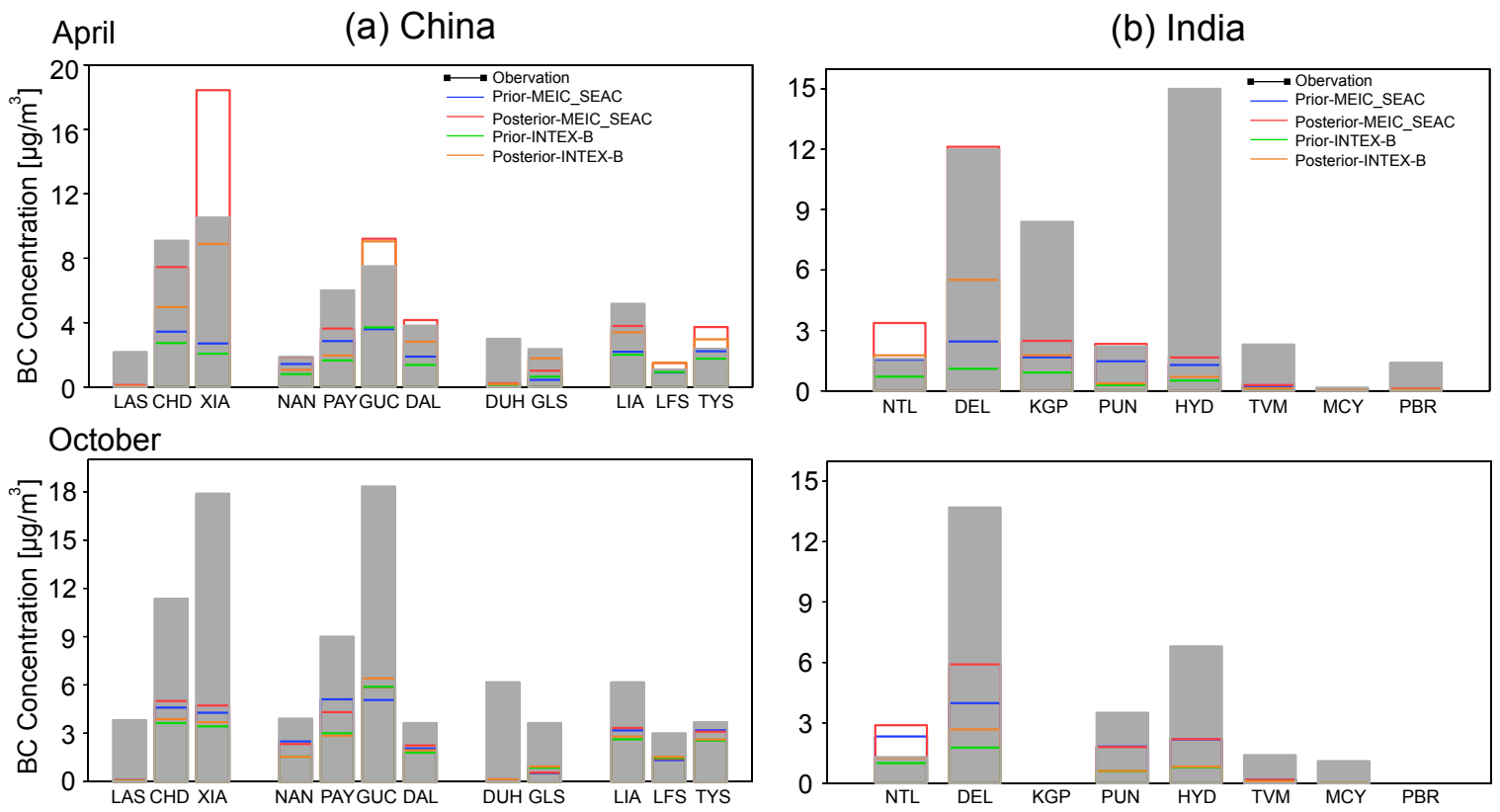


Fig. 18

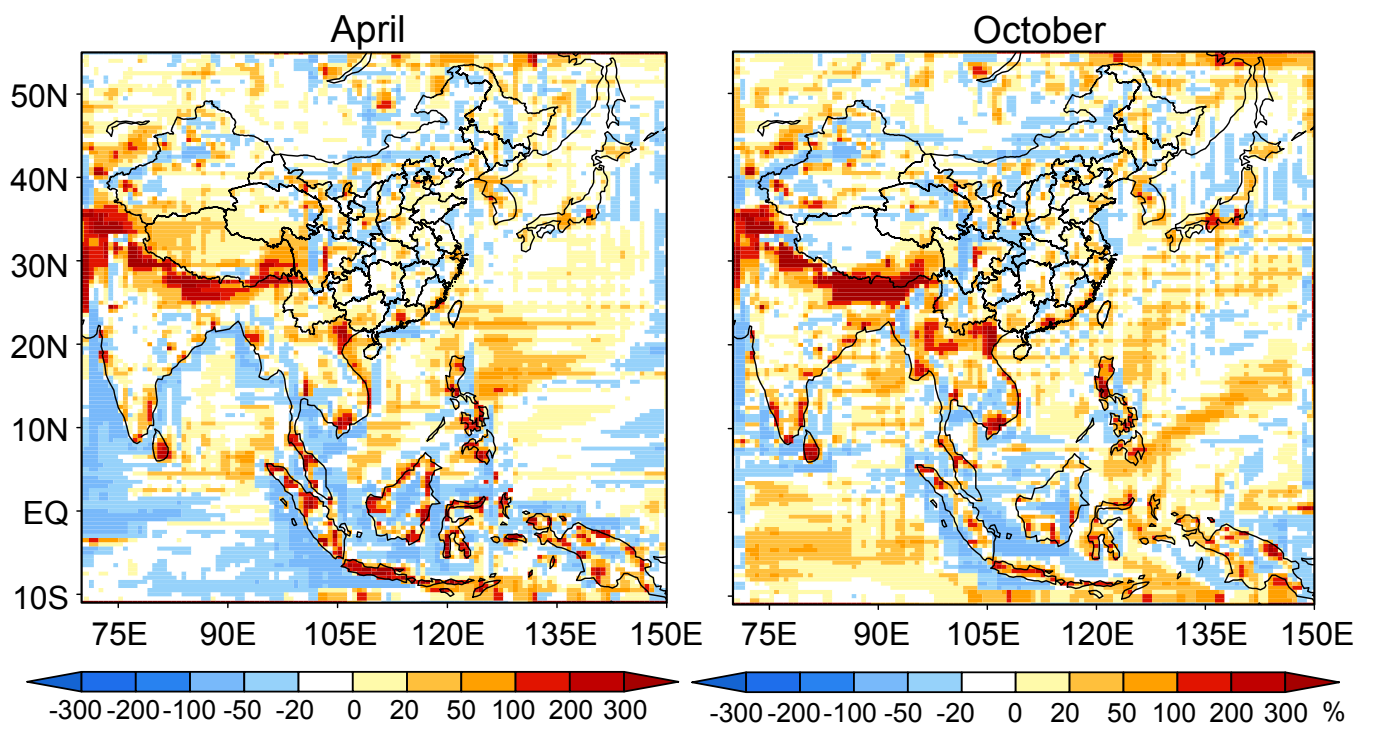


Fig. 19

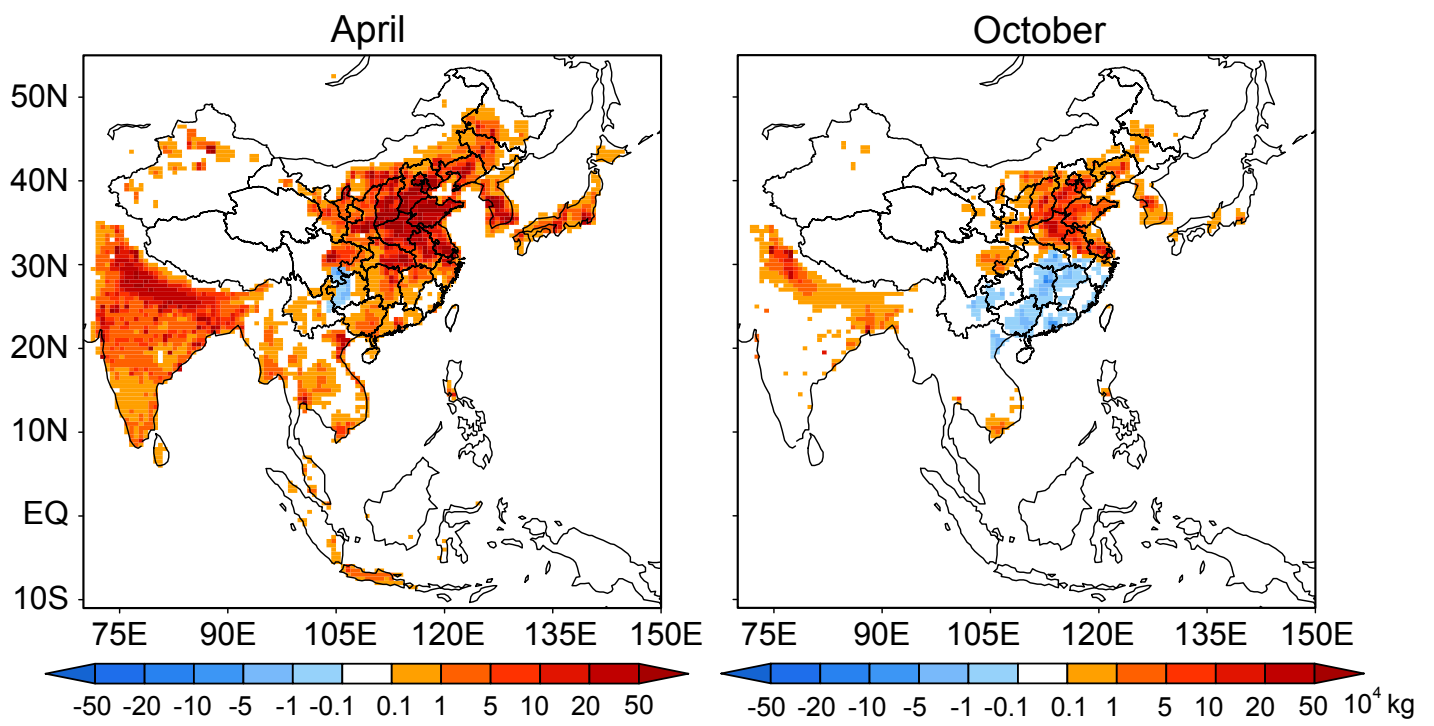


Fig. 20